Draft version February 1, 2008
Preprint typeset using LaTeX style emulateapj v. 04/03/99

PROMPT AND DELAYED EMISSION PROPERTIES OF GAMMA-RAY BURSTS OBSERVED WITH BEPPOSAX

F. Frontera[1,2], L. Amati[1], E. Costa[3], J.M. Muller[4,5], E. Pian[1], L. Piro[3], P. Soffitta[3], M. Tavani[6,7], A. Castro-Tirado[8], D. Dal Fiume[1], M. Feroci[3], J. Heise[4], N. Masetti[1], L. Nicastro[9], M. Orlandini[1], E. Palazzi[1], R. Sari[10]

Draft version February 1, 2008

ABSTRACT

We investigated the spectral evolution in the 2–700 keV energy band of Gamma-Ray Bursts (GRBs) detected by the Gamma-Ray Burst Monitor (GRBM) and localized with the Wide Field Cameras (WFCs) aboard the BeppoSAX satellite before May 1998. Most of them have been followed-up with the Narrow Field Instruments aboard the same satellite. In the light of these results we discuss open issues on the GRB phenomenon. We find that the optically thin synchrotron shock model (SSM) provides an acceptable representation of most of the time-resolved GRB spectra extending down to 2 keV, except in the initial phases of several bursts and during the whole duration of the quite strong GRB970111, where a low-energy photon depletion with respect to the thin SSM spectrum is observed. A strong and time variable low energy cut-off, consistent with absorption effect, is observed during the prompt emission of GRB980329. We find that the X-ray afterglow starts at about 50% of the GRB duration, and that its fluence, as computed from the WFC light curve, is consistent with the decay law found from the afterglow NFI observations. We also investigate the hydrodynamical evolution of the GRB in our sample and their associated afterglow, when it was detected. We find that the photon index of the latest spectrum of the GRB prompt emission is correlated with the index of the afterglow fading law, when available, as expected on the basis of an external shock of a relativistic fireball. We also find that for most of the GRBs in our sample the late emission is consistent with a slow cooling of the shock. Adiabatic shocks appear more likely than radiative shocks. Parameters of the shocks at earliest times have been derived.

Subject headings: gamma rays: bursts — gamma rays: observations — X–rays: general — hydrodynamics: — shock waves

1. INTRODUCTION

In the last two years a big step forward has been accomplished in the GRB astronomy, thanks to the BeppoSAX(Boella et al. 1997a) capability of precisely positioning these events soon after their detection (Piro et al. 1998a). The ensuing discovery of GRB afterglow emission in the X-ray, optical and radio bands has provided the distance for some GRBs and important information on the GRB remnants and their environments, necessary to improve our understanding of the radiation mechanisms and the origin of GRBs. Time averaged spectra of GRBs seem to be consistent with the synchrotron shock model (Tavani 1996), while Inverse Compton emission is expected to operate at very early times (Waxman 1997).

Models of GRBs and afterglow emission are mainly based on mechanisms of dissipation of kinetic energy of a relativistic expanding fireball (Mészáros and Rees 1997, Wijers et al. 1997, Vietri 1997). There

[1]Istituto Tecnologie e Studio Radiazioni Extraterrestri, CNR, Via Gobetti 101, 40129 Bologna, Italy
[2]Dipartimento di Fisica, Università di Ferrara, Via Paradiso 12, 44100 Ferrara, Italy
[3]Istituto Astrofisica Spaziale, C.N.R., Via E. Fermi 21, 00044 Frascati, Italy
[4]Space Research Organization in the Netherlands, Sorbonnelaan 2, 3584 CA Utrecht, The Netherlands
[5]*BeppoSAX* Scientific Data Center, Via Corcolle 19, 00131 Roma, Italy
[6]Istituto Fisica Cosmica e Tecnologie Relative, C.N.R., Via Bassini 15, 20133 Milano, Italy
[7]Columbia Astrophysics Laboratory, Columbia University, New York, NY 10027
[8]Laboratorio de Astrofisica Espacial y Fìsica Fundamental, P.O. Box 50727, 28080 Madrid, Spain, and Instituto de Astrofísica de Andalucía (IAA-CSIC), P.O. Box 03004, E-18080 Granada, Spain
[9]Istituto Fisica Cosmica e Applicazioni all'Informatica, C.N.R., Via U. La Malfa 153, 90146 Palermo, Italy
[10]Theoretical Astrophysics, 130-33, California Institute of Technology, Pasadena, CA 91125, USA

are open issues concerning the production process of the prompt γ-ray radiation (e.g., internal or external shocks of the fireball material, Kobayashi et al. 1997), the time when the afterglow sets in as compared to the end of the prompt GRB emission (Sari 1997), the production process of the delayed radiation (e.g., radiative shock vs. adiabatic shock, see Sari, Piran and Narayan 1998). All these issues require observations.

BeppoSAX offers the possibility to perform in a broad energy band (2–700 keV) temporal and spectral studies of the primary events from which afterglow emission has been detected. Indeed, when an event is simultaneously detected by the Gamma-Ray Burst Monitor (GRBM, 40–700 keV) (Frontera et al. 1997, Feroci et al. 1997) and by one of the two Wide Field Cameras (WFCs, 2-26 keV, Jager et al. 1997), it is possible to obtain, besides a precise localization (few arcmin radius error boxes), also X- and γ-ray spectra and time profiles of the GRBs. Therefore it is possible to study the spectral evolution of GRBs and relate the spectral and temporal properties of the main events with those of the associated X–ray afterglows.

Results on the spectral evolution of GRBs in a broad band were reported by Strohmayer et al. 1998 , using the GRB detections obtained with the Gamma-Ray Burst Detector on board the Ginga satellite. However, due to the lack of knowledge of the GRB direction and thus a poor knowledge of the instrument response function, those results were unavoidably of limited accuracy.

We have already reported on the time averaged spectra of some GRBs observed with the BeppoSAX GRBM and WFCs (Frontera et al. 1998b). In this paper we will concentrate mainly on the evolution of the spectral properties of a sample of GRBs occurred between July 20, 1996 and April 25, 1998. For completeness we include in our sample also GRB960720 and GRB970228, the spectral evolution of which was already studied with results consistent with those obtained with the present analysis (Piro et al. 1998a, Frontera et al. 1998a). Results of comparative spectral analysis of the GRBs detected after April 25, 1998, will be the subject of a future paper.

2. INSTRUMENTATION AND GRB SAMPLE

The GRBM consists of the 4 anti-coincidence shields of the Phoswich Detection System instrument (Frontera et al. 1997, Feroci et al. 1997, Amati et al. 1997). Each shield is a CsI(Na) scintillator slab 10 mm thick with a geometric area of 1136 cm^2. Each slab is open to the sky, except along some directions, where material from other BeppoSAX instruments heavily decreases the transparency of the slab γ-ray entrance window. The GRBM detector operates in the 40-700 keV energy band. Two of the four GRBM units are co-aligned with the WFCs: unit 1 with WFC No. 1 and unit 3 with WFC No. 2. The data available from GRBM for spectral analysis include two 1 s ratemeters (40–700 keV and >100 keV) and 240 channel spectra in the 40–700 keV band integrated over 128 s. For the GRB spectral evolution we use the 1 s ratemeters, but we check their consistency with the GRB time averaged spectra obtained from the 240 channel data(Amati et al. 1999). The energy resolution of GRBM units 1 and 3 with energy has been discussed by Amati et al. (1997) ; e.g., at 279 keV (^{203}Hg line) it is 20%. The on-axis effective area of the GRBM units 1 and 3 is 420 cm^2 in the 40–700 keV band and is 500 cm^2 at 300 keV.

The WFC instrument consists of two coded aperture cameras, each with a field of view of $40^\circ \times 40^\circ$ full width at zero response and an angular resolution of 5 arcmin. WFCs have an energy resolution $\approx 20\%$ at 6 keV, are operated in normal mode with 31 channels in 2–26 keV and 0.5 ms time resolution. The on-axis effective area of WFCs No. 1 and 2 averaged in the 2–26 keV energy band is 118 cm^2 (Jager et al. 1997). The follow-up observations of the GRB error boxes provided by the WFCs are performed with the Narrow Field Instruments (NFIs) aboard BeppoSAX, that are orthogonal to both the WFC and GRBM axes. They include two imaging instruments (LECS, 0.1-10 keV, Parmar et al. 1997; MECS, 2-10 keV, Boella et al. 1997b) and two direct-viewing detectors (HPGSPC, 3-60 keV, Manzo et al. 1997 ; PDS, 15-300 keV, Frontera et al. 1997).

The list of the BeppoSAX GRB events included in our sample is given in Table 1 along with some basic information: position error radius, offset angle of the GRBs with respect to the instruments (GRBM and WFC) axis, peak fluxes and time durations T_X and T_γ in the X–ray (2-26 keV) and γ–ray (40-700 keV) band, respectively, time delay of the first NFI observation from the primary event. Positive or uncertain (indicated by a question mark) X–ray, optical or radio afterglow detection is reported in the last column. The GRB time durations are estimated from the 1 s ratemeters and give the time interval during which the GRB count rate is higher than the estimated background level by at least 2σ. As can be seen, T_X is generally greater or at most equal to T_γ.

3. SPECTRAL ANALYSIS

The light curves from the WFCs and GRBM instruments are shown in fig. 1. Each light curve was divided into a given number of temporal sections (see fig. 1), and a spectral analysis in the 2–700 keV energy band was performed for the average spectrum of each section. The duration of the sections was cho-

sen to be shorter during the rise of the burst in order to study the evolution of the primary event at the earliest times. The spectral analysis was performed following the same procedure used for GRB970228 (Frontera et al. 1998a). The background level was subtracted from the GRB count rates (see fig. 1) as follows. For the GRBM spectra, this level was estimated using the count rates immediately before and after the GRBs. If the background is variable during the GRB, it is estimated by interpolation, using a quadratic function that fits 150 s count rate data before the burst and 150 s data after its end. For the WFC spectra and light curves, the background level is estimated using an equivalent section of the detector area not illuminated by the burst or other known X-ray sources. We also checked the consistency of this background level with that obtained by using the data before and after the burst. The response function of GRBM units 1 and 3 (Amati et al. 1997) is derived from on-ground calibrations and checked with the Crab Nebula that was clearly detected using the Earth occultation technique (Guidorzi et al. 1998). The response function is currently known with an uncertainty of about 10% for incident photons with low offset angles with respect to the instrument axes, as it is the case of the GRBs in our sample (see Table 1). We added in quadrature this uncertainty to the Poissonian variance.

We used XSPEC software package, issue 10 (Arnaud 1996) to deconvolve count rate spectra, assuming a given theoretical model as input function. In the following, all quoted errors correspond to 90% confidence level for each interesting parameter.

A simultaneous fit to the time averaged WFC and GRBM spectra was performed by using as input model a photo-electrically absorbed (Morrison and McCammon 1983) smoothly broken power law (Band et al. 1993) given by:

$$N(E) = Aexp(-\sigma N_H)\left(\frac{E}{100keV}\right)^{\Gamma_X}\exp\left(-E/E_0\right)$$

if

$$(\Gamma_X - \Gamma_\gamma)\cdot E_0 \;\geq\; E$$

and

$$N(E) = A\left[\frac{(\Gamma_X-\Gamma_\gamma)E_0}{100keV}\right]^{\Gamma_X-\Gamma_\gamma}\exp\left(\Gamma_\gamma-\Gamma_X\right)\cdot\left(\frac{E}{100keV}\right)^{\Gamma_\gamma}$$

if

$$(\Gamma_X - \Gamma_\gamma)\cdot E_0 \;\leq\; E$$

where $\sigma = \sigma(E)$ is the photo-electric cross-section of a gas with cosmic abundance (Morrison and McCammon 1983), N_H is the equivalent hydrogen column density to the GRB, Γ_X and Γ_γ are the power law low energy (below E_0) and high energy (above E_0) photon indices, respectively, and A is the normalization parameter.

The derived best fit parameters, N_H, Γ_X, Γ_γ, peak energy E_p of the logarithmic power ($\nu F(\nu)$) per photon energy decade, are shown in Table 2 for each of the temporal sections. The value of E_p is given by $E_p = E_0(2+\Gamma_X)$, under the condition that $\Gamma_\gamma < -2$. The reduced χ^2 values obtained from the best fits were always acceptable (less than 1.1). We also derived lower limits on E_p when the $\nu F(\nu)$ spectrum showed a bending at the γ-ray energies, but with $\Gamma_\gamma > -2$. In this case, E_p was derived under the condition that the fit to the data was still acceptable, assuming a Γ_γ slightly lower than -2 ($= -2.1$). The lower limits on E_p reported in Table 2 were thus obtained from the lower limits on E_0 corresponding to a 90% confidence level.

When the N_H values were not constrained from the data, they were fixed at the Galactic values along the GRB directions, except for GRB980329, for which we adopted the value derived from the late afterglow observation (in 't Zand et al. 1998).

Also reported in Table 2 are the spectral and temporal properties of the associated X–ray afterglows in the 0.1–10 keV energy band as derived from the TOO observations with the NFIs. The two spectral parameters (photon index Γ_a and column density N_H) were derived assuming a photo-electrically absorbed(Morrison and McCammon 1983) power law model with photon index Γ_a, while the parameter δ is the index of the fading law $I(t)\propto t^{-\delta}$, which best fits the 2–10 keV light curve.

4. RESULTS

For three GRBs (GRB960720, GRB970508, GRB980425) the γ-ray emission starts earlier than the X-ray emission, while in the other GRBs γ-rays and X-rays rise simultaneously (fig. 1). Duration and shape of the GRB time profiles change from one GRB to the other, even if some similarity is observed between GRB980329 and GRB980425, while GRB960720 and GRB970508 exhibit strikingly similar light curves. No X-ray precursor activity is detected, similar to that seen in other GRBs by the Gamma Burst Detector (GBD) on-board Ginga (Murakami et al. 1991) or WATCH/Granat (Castro-Tirado et al. 1994).

Time duration and shape of the GRB time profiles change from one GRB to the other, even if some similarity is observed between GRB980329 and GRB980425.

From the low values (<1.1) of the reduced χ^2, we can infer that the GRB spectra of our sample can be described by a Band law (see eq. 1), even if, in some temporal sections (in the case of GRB970402 in both sections), they are single power laws. GRB spectra evolve with energy and with time (see Table 2). The

spectra are generally harder at low energies or they exhibit the same slope at high and low energies. We do not find bursts with low energy excesses with respect to the Band law (see eq. 1) as claimed by other authors (Preece et al. 1996, Strohmayer et al. 1998).
In the first few seconds, during the GRB rise (fig. 1) we find, for 4 GRBs, that the low-energy photon index Γ_X is significantly larger than -2/3, limit slope of the low energy tail of the instantaneous energy spectrum of an optically thin synchrotron emission (see Section 5.1). This feature was already noticed for GRB960720 (Piro et al. 1998a). In one case (GRB970111) it holds for the entire GRB duration.
The spectra are generally softer during the tail of the GRBs. A remarkable exception is observed in the spectrum of GRB970228, that shows a softening during the first pulse, but it becomes harder during the subsequent minor pulses of the event tail (see fig. 1). This feature was already discussed by Frontera et al. (1998a) .
If we compare the GRB photon index Γ_X during the GRB tail with the photon index Γ_a of the power law spectrum of the associated X-ray afterglow, when available, it can be seen that the afterglow spectrum is generally softer than the GRB tail spectrum.
Generally the absorption column densities are consistent with the Galactic values along the GRB directions, except for GRB980329. In this case, the N_H values are higher than the Galactic value ($0.94\times 10^{21}\,cm^{-2}$) in the temporal sections from A to F, while in the last two temporal sections (G and H), we are not capable to constrain the N_H value, that was frozen to the value estimated during the late afterglow observation (in 't Zand et al. 1998), but was also consistent with the Galactic value. A much higher hydrogen column density (about $1\times 10^{23}\,cm^{-2}$) is specially apparent during the section E corresponding to the early decay of the primary event (see fig. 1 and Table 2).
The $\nu F(\nu)$ spectrum in each of the temporal sections in which we subdivided the time profiles of the GRBs in our sample is shown in fig. 2. The evolution of the peak energy E_p is apparent for most of the GRBs studied. As an example, GRB970228 shows a peak energy quickly crossing the 2–700 keV passband during the first peak, while the peak energy of GRB970111 is still within that energy range until the end of the event. There is no evidence of softening in the spectra of GRB970402, but from the slope of the $\nu F(\nu)$ spectrum (see fig. 2), it is clear that E_p is above 700 keV. GRB980425, presumably associated with the supernova SN 1998bw (Galama et al. 1998b), does not show special features with respect to the other GRBs in our samples: its peak energy decreases with time from the GRB onset.
The GRB970111 behavior deserves particular attention. The X-ray spectral shape is unchanged, while the γ-ray spectrum steepens monotonically. This indicates a progressive decrease of E_p, which however almost stabilizes at 30-40 keV starting about 23 s after the GRB onset. This result is better apparent in fig. 3, that shows the time behavior of Γ_X as a function of Γ_γ for all GRBs considered. When the peak energy is above or below the 2–700 keV passband, we would expect to measure approximately similar photon indices Γ_X and Γ_γ (see Section 5.3) and the value of (Γ_X, Γ_γ) should be along the diagonal (dashed line in fig. 3). On the contrary, Γ_X and Γ_γ could be markedly different (with Γ_X close to the limit value -2/3 for an optically thin synchrotron spectrum) when E_p is in the 2–700 keV passband. In this case (Γ_X, Γ_γ) should lie out of the diagonal. If E_p, during the primary event, sweeps the above passband, the plot of (Γ_X, Γ_γ) should start on the diagonal, go away from it and go back on the diagonal. In the case of GRB970111 E_p enters the 2–700 keV passband soon after the onset, but does not completely cross it until the end of the GRB. In some cases (GRB960720, GRB970228) it sweeps 2–700 keV passband, while in other cases (GRB971214, GRB980329, GRB980425) the peak energy is still in the passband at the end of the primary event. In the case of GRB970402, from the rising of its $\nu F\nu$ spectrum (fig. 2), the peak energy is clearly above 700 keV, while for GRB970508 there is a hint that E_p crosses the 2–700 keV passband.
In only one case (GRB971214) we observe a hardening in the afterglow spectrum with respect to that observed during the prompt emission as expected in the model discussed by Waxman (1997) .

5. DISCUSSION

We discuss our results in the light of current theories on GRBs in order to contribute to solve many open issues concerning the GRB phenomenon.

5.1. *Test of the Synchrotron shock model*

As discussed by several authors (see, e.g., Katz 1994, Tavani 1996, Sari & Piran 1997b), the electromagnetic radiation from GRBs and their afterglows is likely due to synchrotron radiation from accelerated particles in internal or external shocks of a relativistically expanding fireball (Synchrotron Shock Model, SSM). The observed hard-to-soft change of the spectrum with energy and with time from the GRB onset is in agreement with this picture (Dermer, Bőttcher and Chiang 1999).
Assuming that the emission region is optically thin, the expected power law index of the $\nu F(\nu)$ spectrum below the peak energy E_p is expected to be in the range from 1/2 to 4/3 (corresponding to -3/2 to -

2/3, respectively, in the photon spectrum), where the first index is obtained when cooling of the particle distribution during the GRB is also taken into account, while the latter index is reached in the case of an instantaneous spectrum or for monochromatic particles (Cohen et al. 1997). Notice that the limit of -2/3 is independent of the electron distribution or uniformity of the associated magnetic field.

As discussed by Tavani (1996) , the Band law is a good approximation of the spectrum expected by the thin SSM and our results confirm this fact. However, using this simple model, we find that, for 50% of the GRBs (see fig. 4), Γ_X is above the expected limit photon index (-2/3) in the earliest time intervals of the light curve. In the case of the intense GRB970111, this holds almost for the entire GRB duration. Crider et al. (1997) found a similar violation in the 30-1800 keV spectra of GRBs observed by BATSE, while Strohmayer et al. (1998) and Preece et al. (1998) find this violation in time averaged spectra of GRBs detected with the GBD/Ginga and BATSE/CGRO experiments, respectively.

Our data confirm that some additional mechanism is certainly active for some GRBs, that modifies the optically thin synchrotron spectrum at very early times. This could be synchrotron self-absorption(Papathanassiou 1999), Compton up-scattering of low-energy photons (Liang et al. 1997) or plasma physics effects (Tavani 1999). Assuming single Compton up-scattering by highly relativistic electrons with random direction, the limit photon index of the low-energy spectrum is zero (Rybicki and Lightman 1979). We find that the low-energy photon index of all GRBs in our sample, except that of GRB970111, is consistent with this limit value.

The approximate stabilization of E_p at $\sim$35 keV for GRB970111, corresponding to a decrease of the power law photon index Γ_γ will be discussed in Section 5.3.3. For the other GRBs, the change of the photon index observed starting from the GRB tail up to the late X-ray afterglow observations not as much relevant.

The high N_H observed during the prompt emission of GRB980329 and its decrease during the tail of the event can be interpreted in two ways. It might be a consequence of variable absorption of external intervening material due to its progressive photoioniziation as the GRB evolves (Bőttcher et al. 1998). In this case Bőttcher et al. (1998) also expect fluorescence features and/or K edges that are not apparent in the prompt and delayed emission (in 't Zand et al. 1998). However these features could be too weak to be detectable with our instruments and/or could be not within the WFC or NFI passband, due to the redshift. The redshift of GRB980329 is still unknown (see a possible estimate in Fruchter 1999) . The other possibility is that intrinsic absorption takes place at the GRB site. If this is the case, in the context of the fireball shock model (Sari, Piran and Narayan 1998), N_H is given by $E/(\gamma_0 m_p c^2)$ divided by $4\pi r^2$, where E is the energy of the shock, γ_0 is initial Lorentz factor of the shocked material, m_p is the proton mass, c is the light velocity ad r is the distance from the explosion center to the shock dissipation radius. With typical values for the energy E ($\sim 10^{52}$ erg) and γ_0 ($\sim$ 100), the measured N_H gives a value of r$\sim 10^{14}$ cm, which is inconsistent with external shocks that are expected only at values of R$\sim 10^{16}--10^{17}$ cm, when the N_H would be lower by a factor of 10^4-10^6. Thus our results points rather to internal shocks accompanied by rapid expansion of a fireball.

5.2. *Earliest X-ray afterglow emission*

Table 3 shows the X-ray (2-10 keV) and γ-ray (40-700 keV) fluences, S_X and S_γ, of the GRBs in our sample as derived from our spectral analysis. For comparison, when available, also the 2-10 keV fluence S_a of the afterglow emission is given. The latter was estimated from the fading laws (see Table 2) integrated over the time interval from the GRB end up to 10^6 s, when the X-ray afterglow emission level is generally already negligible for a power slope δ of the fading law greater than 1, as in our case. The ratio S_X/S_γ changes from event to event and ranges from 1% to about 40%. It does not seem that detection of X-ray afterglow emission is related to the amplitude of the above ratio. Also the ratio S_a/S_γ changes from a GRB to another, ranges from 0.4% to about 20% and does not appear to be strictly related with the S_X/S_γ value, as also evident from the S_a/S_X ratio. This ratio also shows that the fluence of the X-ray afterglow emission is, within a factor 2, of the same order of that measured, in the same energy band, during the primary event.

In the scenario of the fireball model, in order to explain the complex time profiles of GRBs, it was shown (Kobayashi et al. 1997, Sari and Piran 1997b) that the GRB main event could be due to internal shocks, although for simple fast-rise/exponential-decay (FRED) events also external shocks can be accepted (Dermer, Bőttcher and Chiang 1999). Instead, there is general consensus that the GRB late afterglow emission is likely due to the external shocks propagating in the interstellar medium (Mészáros and Rees 1997, Sari, Piran and Narayan 1998). In this scenario, the two phenomena can evolve in different ways and can involve energetics not necessarily correlated. However it has been suggested (Sari 1997, Sari and Piran 1999b) that the early afterglow could start few dozens of seconds after the burst. We tested this

prediction for the GRBs in our sample. We have already shown (see, e.g., Costa et al. 1998 and Piro et al. 1998) that the extrapolation of the 2-10 keV afterglow fading law back to the time of the GRB is in agreement with the 2-10 keV flux measured during the last portion of the event. This should suggest that at least the tail of the GRBs could be due to afterglow emission, while at the beginning of the primary event, the contribution to the GRB emission from the afterglow is negligible. We adopt the following procedure to perform the test. It is reasonable to assume that the intensity of the X-ray afterglow depends on the spectral index Γ_a and temporal index δ according to the following law:

$$I(E,t) \propto E^{\Gamma_a} t^{-\delta} \quad (1)$$

With this assumption, the more general expression of the ratio between the 2–10 keV fluence in the time intervals (t_1, t_2) and (t_2, ∞), with $t_2 > t_1$, is given by

$$R(t_1,t_2) \equiv S(t_1,t_2)/S(t_2,\infty) = K(\bar{\Gamma}_1,\bar{\Gamma}_2)[(t_1/t_2)^{-\delta+1}-1] \quad (2)$$

where S(t_1,t_2) is the 2-10 keV fluence in the (t_1,t_2) interval, S(t_2,∞) is the fluence in the interval from t_2 to a time $t \gg t_2$ where the afterglow intensity has decreased to a negligible value, $\bar{\Gamma}_1$ and $\bar{\Gamma}_2$ are the average photon indices of the afterglow power law spectral emission in (t_1, t_2) and (t_2, ∞), respectively. Notice that parameter $K(\bar{\Gamma}_1,\bar{\Gamma}_2)$ must be greater than 1 if the spectrum becomes softer with time as observed (see Table 2).

If we express t_1 and t_2 in terms of the time duration T of each GRB, that is, $t_1 = f_1 T$ and $t_2 = f_2 T$, with $f_1 < f_2$, the previous equation becomes

$$R(f_1,f_2) = K(\bar{\Gamma}_1,\bar{\Gamma}_2)[(f_1/f_2)^{-\delta+1}-1] \quad (3)$$

The ratio R(f_1,f_2) for each GRB of our sample was evaluated assuming $f_2 = 1$ and different values of f_1. The result obtained for $f_1 = 0.01$ and $f_1 = 0.63$ is shown in fig. 5. The above law gives a good fit to the data ($\chi^2_\nu = 1.04$, dof=4) in the case $f_1 = 0.63$, but an unacceptable fit ($\chi^2_\nu = 2.5$, 4 dof) in the case $f_1 = 0.01$ when the total GRB fluence is used. We also checked the behavior of the above ratio in the case $f_1 = 0.40$, obtaining a reduced $\chi^2_\nu = 1.3$. In fig. 5 (bottom panel) we show the best fit curve, with K = 1.66±0.36, in the former case. For comparison, the curve with K=1, under the assumption of no spectral evolution from (t_1, t_2) to (t_2, ∞), is also shown. In fig. 5 (top panel), we report the expected curve with the minimum value of K allowed (K=1) in the case $f_1 = 0.01$. There is no agreement between data and expected dependence of R(0.01,1) on δ.

This result shows that roughly the second half of the GRB X-ray light curve is consistent with afterglow emission. Likely GRB time profiles are the superposition of two components, one due to the process that produces the main event and the other due to the delayed emission. A possible scenario envisages the former component as due to internal shocks and the latter due an external shock (see, e.g., Sari (1997)). If the emission due to internal shocks has a short duration, the afterglow can be separated from the internal component, that gives rise to the earliest emission of a GRB. This could be the case of GRB970228(Costa et al. 1997, Frontera et al. 1998a), in which the first peak (see fig. 1) could be due to an internal shock, while the late emission could be due to external shocks and thus coincide with the afterglow emission.

According to the internal-external shock model for the GRB, from the above results, it is possible to evaluate the initial Lorentz factor γ_0 of the shocked fluid (Sari and Piran 1999a, Sari and Piran 1999b):

$$\gamma_0 = 240 E_{52}^{1/8} n_1^{1/8} (t/10\ s)^{-3/8} \quad (4)$$

where t is the onset time of the afterglow emission, E_{52} is the afterglow energy released in the shock in units of 10^{52} erg and n_1 is the number density of the ambient medium in units of cm^{-3}. If the early afterglow starts at about 50% of the GRB duration, for those GRBs for which it is possible to make an estimate of E_{52} (see Table 3), we obtain the values of γ_0 reported in Table 4, assuming a constant ambient medium density $n_1 = 1$. The luminosity distance was evaluated from the redshift values reported in Table 3, assuming a standard Friedman cosmology with $H_0 = 65$ km/s/Mpc and $\Omega = 0.3$. The energy released was assumed to be isotropic. The value of γ_0 is of the order of 150 for all GRBs in our sample with known distance, except for GRB980425. For this peculiar GRB, we have assumed its coincidence with the type Ic supernova SN1998bw (Galama et al. 1998b). In this case, Pian et al. 1999b estimate an afterglow emission with fading law index $\delta > 1.3$. This upper limit was obtained assuming that the afterglow starts during the GRB tail as discussed above, and considering only the first TOO measurement as main contribution to the afterglow radiation, while the radiation detected about 6 months after the main event was assumed to be mainly due to thermal emission from the supernova. The much lower value of γ_0 (< 50) obtained for this GRB shows that the association of GRB980425 with SN1998bw implies a deviation from the extreme relativistic conditions expected for GRBs in the context of the fireball scenario and thus that it could be a member of another class of GRBs. Assuming that this event is not associated with SN1998bw, but with a fireball with redshift $z \sim 1$, we could ob-

tain a value of γ_0 consistent with the values found for the other GRBs.

5.3. *Hydrodynamical evolution of a shock*

An observational test of the hydrodynamical evolution of GRB primary events and afterglows is of key importance to understand the GRB phenomenon. The afterglows evolution resulting from forward shocks with the interstellar medium (ISM) was theoretically investigated by several authors(Sari, Piran and Narayan 1998, Mészáros and Rees 1997, Mészáros and Rees 1999), while the GRB evolution is less clear, except the case of FRED (fast rise, exponential decay) events(Dermer, Bőttcher and Chiang 1999). Here we test the expectations of the model by Sari, Piran and Narayan (1998) making use of our spectral results. This model considers a spherical shock that propagates in a surrounding medium (interstellar medium, ISM) of constant density. The electrons accelerated in the shock are assumed to have a power law distribution of Lorentz factor γ_e ($N(\gamma_e) \propto \gamma_e^{-p}$) where $\gamma_e = E_e/m_e c^2 \geq \gamma_m$ and electron distribution index $p > 2$. Two extreme cases of hydrodynamical evolution of the shock are considered: a fully adiabatic and a fully radiative evolution. In the case of an adiabatic evolution the internal energy of the shock is constant, while in the other case it varies with the bulk Lorentz factor γ. The time dependence of γ is different in the two regimes.

5.3.1. *Late GRB spectrum vs. afterglow decay*

If the GRB tail is due to afterglow emission and thus to an external shock, we should also expect a correlation between spectral properties of the GRB tail and power-law index δ of the fading afterglow emission. The model by Sari, Piran and Narayan (1998) predicts the occurrence of two breaks in the synchrotron spectrum, one at energy E_m corresponding to the lowest energy of the injected electrons with Lorentz factor γ_m, and the other at energy E_c (cooling break), corresponding to the electron energy with Lorentz factor γ_c, above which cooling for synchrotron radiation is significant. Figure 6 shows the expected evolution of the $\nu F(\nu)$ spectrum for fully adiabatic and fully radiative cooling of the shocks, for typical values of the model parameters (see values in the figure caption). Due to the different variation with time of E_c and E_m (see Sect.5.3.2), at early times, $E_m > E_c$ (fast cooling), while at late times, $E_m < E_c$ (slow cooling). The passage from fast cooling to slow cooling occurs at a time t_0 when $E_m = E_c = E_0$. It was shown (Sari, Piran and Narayan 1998) (see also fig. 6) that the expected power law photon index of the afterglow spectrum is given by -3/2 for $E_c < E < E_m$ and by -p/2-1 in the high energy tail (E higher than E_m and E_c), independently of the cooling mechanism of the shock (radiative or adiabatic). From Fig. 2 and its comparison with fig. 6, we can see that, in the case of GRB970228 and GRB970402, the high energy photon index Γ_γ^l of the last section of the time profiles is consistent with -3/2, while for the other GRBs in our sample it is likely related with the high energy tail of the associated afterglow. We make this assumption setting, for all GRBs in our sample except GRB970228 and GRB970402, $\Gamma_\gamma^l =$ -p/2-1.

The fading law of the 2-10 keV afterglow emission ($I(t) \propto t^{-\delta}$) provides a further relation between p and δ. Indeed the model by Sari, Piran and Narayan (1998) expects that the index δ is related to p through $\delta = 3p/4 - 1/2$ in the case of an adiabatic cooling of the shock when both E_m and E_c are below the 2–700 keV passband at the epoch t of the afterglow observation. This is likely our case. The same model expects that, in the case of a radiative cooling of the shock (in this case the shock becomes adiabatic at time t_0 when $E_m = E_c$), $\delta = 6p/7 - 2/7$. Combining all the above relations, we found the following dependence of Γ_γ^l on δ: $\Gamma_\gamma^l = -4/3 - 2/3\delta$ for an adiabatic shock, and $\Gamma_\gamma^l = -7/6 - 7/12\delta$, for a radiative shock.

The measured values of Γ_γ^l as a function of δ are shown in fig. 7a. Superposed to the data are the curves derived from the above relations. For comparison, we show in Fig. 7b, for all GRBs in our sample for which the afterglow spectrum is known, the power-law photon index Γ_a of the X-ray afterglow (see Table 2) as a function of the corresponding index δ of the fading law in the same energy band. Also shown in the figure are the expected Γ_a vs. δ relationships (Sari, Piran and Narayan 1998): $\Gamma_a = -7/6 - 7/12\delta$ for radiative cooling ($t < t_0$), while for an adiabatic cooling, $\Gamma_a = -2/3\delta - 1$ or $\Gamma_a = -2/3\delta - 4/3$, depending on the observing time t after the primary event, if $t_m < t < t_c$ or $t > t_c$, respectively. The parameters t_m and t_c are the times at which E_m and E_c sweep the energy passband of the MECS detectors, respectively (see fig. 6).

From fig. 7a, it appears that the data are consistent with the expected dependence of Γ_γ on δ, but their uncertainties do not allow us to discriminate among different cooling models. The peculiarities of GRB970111 and GRB980425 are also apparent from this plot. Assuming that the afterglows associated with these GRBs satisfy one of the two plotted relationships, the X-ray afterglow of GRB970111 should have exhibited a fading law with power-law index lower than -2, that is consistent with its non detection with BeppoSAX 17hrs after the primary event. The same condition applied to the GRB980425 afterglow

implies a much lower δ than -2.
Also the measured Γ_a vs. δ are consistent with the expected relationships between these two quantities derived from the synchrotron shock model(Sari, Piran and Narayan 1998), but, also in this case, due to the uncertainties in these parameters, we cannot discriminate among different cooling laws.

The above discussed δ vs. p and Γ vs. p relationships have also permitted the estimate of the index of the electron distribution for 5 GRBs in our sample. Given the lower uncertainty in the value of δ (see Table 2), we report in Table 4 the values of p derived from δ. We assume an adiabatic cooling (see sect. 5.3.2) in the two cases above considered (t_m <t<t_c, and t>t_c). The corresponding values of p derived from Γ_a, due to the larger uncertainty in this parameter (see Table 2) are consistent with the p values reported in Table 4. These change from one GRB to the other and rage from 2.1 to 3.1. It is remarkable that for the two GRBs (971214 and 980329) for which it was possible to derive the values of p from the spectral index Γ_γ^l of the prompt emission, we found values of p also consistent with those reported in Table 4 (3.2±1 for GRB971214 and 2.6±0.6 for GRB980329).

5.3.2. *Temporal evolution of the peak energy E_p*

As shown in fig. 6, the model by Sari, Piran and Narayan (1998) predicts a temporal evolution of the $\nu F(\nu)$ spectrum of the GRB afterglow. A spectral evolution is also expected during the primary event, even if the time behavior can be more complex: it can change from one GRB to the other and can depend on the assumed model (e.g., external shocks, Dermer, Bőttcher and Chiang 1999 vs. internal shocks, Sari 1997). We observed both spectral evolutions (see Table 2 and fig. 2): on the basis of the results discussed in the previous sections, the spectra obtained in the first half of the GRB duration are mainly due to the primary event, while those obtained later are likely due to afterglow emission (see Sect.5.3.1).
To characterize the spectral evolution, we consider the time behavior of the peak energy E_p of the $\nu F(\nu)$ spectrum. The model by Sari, Piran and Narayan (1998) predicts the occurrence of a maximum in the $\nu F(\nu)$ spectrum in correspondence of one of the two breaks in the synchrotron spectrum, at energies E_m and E_c, respectively (see Sect.5.2). These parameters decrease with time in a different manner and according to the assumed cooling type of the shock (adiabatic or radiative). At early times from the afterglow onset (t<t_0) the peak energy E_p is coincident with E_m that decreases as $t^{-3/2}$ for adiabatic shock and as $t^{-12/7}$ for a radiative shock, while at late times (t>t_0) it is coincident with E_c that decreases as $t^{-1/2}$ for an adiabatic shock and as $t^{-2/7}$ for a radiative shock (see fig. 6). As discussed above, at the time t_0 E_m coincides with E_c (and with E_p). This time is different for an adiabatic or a radiative cooling (see, e.g., fig. 6). Notice that these temporal dependences of E_m and E_c hold during the decay phase of the afterglow, while at the beginning of the fireball interaction with the ISM one expects a shallower decay of the break energies.
Thus the observed time behavior of E_p can constrain the cooling mechanism of the shock and provide the value of important physical parameters, like the fraction ϵ_e of shock energy that goes into the electrons and the fraction ϵ_B that goes in magnetic energy density (Sari, Piran and Narayan 1998).
Figure 8 shows the behaviour of E_p with respect to time for all GRBs in our sample. The values are not corrected for GRB redshift, even when this is known. We have verified that this correction is not critical for our conclusions. For the GRBs with detected late afterglow, we also show in fig. 8, when available, the values of E_p obtained from the literature (GRB970228, Masetti et al. 1999 ; GRB970508, Galama et al. 1998a ; GRB980329, Palazzi et al. 1998 ; GRB971214, Dal Fiume et al. 1999 , Ramaprakash et al. 1998). Superposed to the data is also the expected time behavior of E_m for short times from GRB onset in both the radiative and adiabatic conditions of the shock. In addition we show the behavior of E_c when afterglow emission is detected and the spectrum is known. The E_m curves are normalized to the earliest measured values of E_p, while the E_c curve is normalized at the value of E_p obtained from the late afterglow spectrum. In fig. 8 the time at which the afterglow is expected to have already started (see Sect.5.2) is also shown (vertical dashed line).

For most of the GRBs in our sample, only lower limits of E_p are available in the earliest part of the event. In spite of that, it is apparent that E_p decreases with time more quickly than expected in the case of a fast cooling (adiabatic or radiative) of an external forward shock. This is another evidence for internal shocks during the first part of GRBs.
Another important feature of the data is that, for GRB970228 and GRB970508, the extrapolation of the fast cooling curves at late times is clearly inconsistent with the value of E_p measured during the afterglow about 10 days after the primary event. This means that a transition from a fast cooling to a slow cooling phase of the shock has occurred in the meantime. For GRB970508 we report in fig. 8, in addition to the late value of $E_p \equiv E_c$, the estimated value of E_m (Galama et al. 1998a). This break fits nicely with the adiabatic evolution curve, confirming the passage of the shock from fast to slow cooling. The backward extrapolation of the expected behavior of E_p normal-

ized to the last data point allows us to derive the transition time t_0 from fast cooling to slow cooling. The t_0 values obtained are reported in Table 4, along with the rough estimate of the same parameter for other two GRBs (GRB971214 and GRB980309), for which the transition time t_0 is more uncertain.

The E_p behavior alone does not permit us to clearly establish whether at early times the shock cooling is adiabatic or radiative. We obtained this information by comparing the maximum of the energy spectra F_{max} at early time (during the latest section of GRB time profiles) with that at late time (during late afterglow observations). The results are shown in Table 4. In the case of GRB970508 and GRB980329, F_{max}(early) and F_{max}(late) are comparable, while in the case of GRB971214, F_{max}(early) is a factor from about 4 to 18 higher than F_{max}(late). This range is due to the uncertainty in the true value of F_{max}(late). The two values reported in Table 4 are those given by Ramaprakash et al. (1998) and Dal Fiume et al. (1999) , respectively. The difference is due to the different absorption by dust assumed by these authors to correct the measured magnitudes. Dal Fiume et al. (1999) assumes the extinction typical of starburst galaxies and take into account the redshift of the measured radiation, while Ramaprakash et al. (1998) assume an exponential absorption with optical depth from extinction $\propto 1/\lambda$, where λ is the wavelength of the observed radiation.

As a result, at early times, for GRB970508 and GRB980329, we see an adiabatic evolution of the shock, while for GRB971214, the shock cooling is close to be adiabatic if we assume the highest value of F_{max}(late). As discussed by Dal Fiume et al. (1999) , there are reasons to prefer their correction, which implies that the shock is almost adiabatic.

Also the values of the shock parameters ϵ_e and ϵ_B are reported in Table 4. In the case of GRB970228, we are not able to estimate F_{max}(late) from the available data (Masetti et al. 1999). For this GRB we report the values of these parameters for both a radiative and an adiabatic fast cooling. It is noterworthy that the derived ϵ_B(late) and ϵ_B(early) are roughly in agreement and that they are lower than ϵ_e. This is expected when the contribution from Compton up-scattering cannot be neglected. The value of t_0 derived by us for GRB970508 is consistent with the value (about 700 s) derived by Galama et al.(1998a), who also noticed that an adiabatic model fits better the late afterglow data.

5.3.3. *The peculiar behavior of GRB970111*

We already have discussed in Sections 4 and 5.1 some peculiarities of GRB970111. This GRB stands out for its low energy spectral slope, that is not consistent with a thin synchrotron model and with Inverse Compton, making self-absorption a possible explanation. GRB970111 is also peculiar for its E_p time behavior: a transition in the rate of E_p decrease is observed in correspondence of the expected starting time of the afterglow emission (see fig. 8). However this break cannot be interpreted as passage of the cooling break E_c through the 2-700 keV passband, since the change of the spectral slope above and below E_c is predicted to be 1/2 and we see a much greater change. It therefore must be E_m which should however decrease as $t^{-3/2}$ in the adiabatic case or faster (as $t^{-12/7}$) in the radiative case. Instead the slope of E_p is consistent with $t^{-1/2}$ that is not in agreement with the decay phase of the afterglow.

The evolution of the shock does not appear to be adiabatic. The non adiabatic character is apparent from the time behavior of F_{max}. In the second half of the GRB time profile, the energy spectrum shows an intensity maximum that decreases with time according to a power law with index 2.6, while a constant intensity is expected for an adiabatic cooling. The measured slope is also inconsistent with a radiative cooling, in which case a much lower slope (-3/7) is expected for the power law time decay of F_{max}. The extrapolation of the time behavior of E_p and F_{max} at the time of the first BeppoSAX observation yields X-ray fluxes that are well below the upper limit given by Feroci et al. (1998) . Also the upper limits of the afterglow given in the optical band (Gorosabel et al. 1998) are well above this extrapolation.

A possible intepretation of this strange E_p behavior is that we are observing two successive electron acceleration episodes, giving rise to the first and the second pulses (see γ-ray time profile in fig. 1). During the first pulse, E_p is supposedly decaying but never enters the 2–700 keV passband (as soon as injection stops the peak can sweep this energy band faster than allowed to observe with our time integration of the spectra), while during the second pulse the electron distribution has a long cooling timescale that makes the peak almost stable at around 35 keV. This second episode (that could also be originated by an external shock) should show a roughly constant bulk Lorenz factor that later decays and gives all the power dependences on the lightcurve. Following this interpretation, the electron power law dependence on Γ_γ is p= 1 -2Γ_γ for the early portions of the second pulse and p= -2(Γ_γ+1) for the later ones (Sari, Piran and Narayan 1998). From the measured values of Γ_γ we find, for the second pulse of the GRB, p$\sim$4. This electron index can account for the non detection of X-ray/optical afterglow emission about 13 hrs after the primary event.

6. CONCLUSIONS

Several conclusions can be drawn from the above results. The optically thin synchrotron model (e.g. Tavani 1996) appears to be consistent with the GRB spectra reported in this paper. It can describe most of them and their evolution with time and energy, but not the low energy spectra at earliest times after the GRB onset, where there is a deviation from its expectations. Some additional ingredient, probably self-absorption or Compton up-scattering, is required to explain the low energy spectra at early times. In the case of GRB970111, the deviation is the largest and lasts for the entire GRB duration.

In one case, GRB980329, a relevant and variable absorption has been detected during the prompt emission. This feature appears to be consistent with variable self-absorption of the X-ray emission produced in internal shocks of a relativistic expanding fireball, but absorption from external material that progressively becomes photo-ionized by the GRB radiation cannot be excluded.

The fluence of the second half of GRB time profiles is consistent with that expected from afterglow emission. With this assumption, in the context of the fireball shock model (e.g. Sari, Piran and Narayan 1998), we have derived the initial Lorentz factor γ_0 of the shocked material for 5 GRBs in our sample, for which the redshift has been determined. The value of γ_0 is about 150 for all these events, except for GRB980425 if this GRB is associated with the supernova SN1998bw. In this case we find an upper limit $\gamma_0 < 50$, that is lower than the typical values assumed in relativistic expanding fireballs. This GRB could be a member of another class of events.

We have tested the presence of a correlation between photon index of the late energy spectra of the GRB prompt emission and index of the fading law of the associated afterglow. We find that this correlation exists and it is consistent with the hydrodynamical evolution of an external shock as discussed in the model by Sari, Piran and Narayan (1998). However the uncertainty in the data does not allow the discrimination between different types of evolution (adiabatic vs. radiative, fast cooling vs. slow cooling).

The shock cooling properties have been investigated from the temporal behavior of the peak energy of the $\nu F(\nu)$ spectrum. We have still assumed the external shock model by Sari, Piran and Narayan (1998) . We find that the values of E_p measured in the first half of the GRB time profile have a time behavior which is not consistent with an external shock and confirm that internal shocks have a key role in determining the GRB spectral evolution at earliest times.

Comparing the values of E_p in the second half of the event with those extimated at late times ($\sim 10^6$ s from the GRB onset) when available, we find that for most of these events, a transition from a fast cooling to a slow cooling has taken place. Adiabatic evolution seems to be preferred. In the case of GRB971214, the uncertainty in the peak flux of the afterglow spectrum does not allow the evolution to be determined, although an almost adiabatic evolution is preferred.

We also have determined the fractions of the shock energy that go in electrons and magnetic energy, and the index p of the electron distribution accelerated in the shock. We find that p changes from one GRB to the other and ranges from about 2.1 to 3.1, for an adiabatic shock cooling.

The case of GRB970111 merits particular consideration. From this GRB no afterglow emission was detected about 17 hrs after the primary event. The GRB time profile in the 40-700 keV energy band shows two main pulses, with the second one that occurs in the second half of the GRB duration. We find that the time behavior of the peak energy of the $\nu F(\nu)$ spectrum shows a break in correspondence of the rise of this pulse. If we assume for this GRB what we found for other GRBs with known afterglow emission, this second pulse could be due to an external shock. However the time behavior of E_p is not consistent with that expected during the decay phase of the fast cooling of a spherical shock. A possible interpretation, in the context of an external shock of a fireball model, is that during the second pulse we are observing the phase in which the Lorentz factor of the shocked material is still constant or is decreasing very slowly. The value of p found for this GRB is about 4, that justifies its non detection 17 hrs after the primary event.

We are very grateful to Hara Papathanassiou for very useful comments and suggestions on the manuscript. This research is supported by the Italian Space Agency ASI

REFERENCES

Amati, L. et al. 1997, SPIE Proceedings, 3114, 176
Amati, L. et al. 1998, Nucl. Phys. B (Conf. Proc.), 69, 656
Amati, L. et al. 1999, A&AS, 138, 403
Arnaud, K.A. 1996, Astronomical Data Analysis Software and Systems V, eds. Jacoby, J. and Barnes, J., ASP Conf. Series 101, 17.
Band, D. et al. 1993, ApJ, 413, 281
Boella, G. et al. 1997a, A&AS, 122, 299
Boella, G. et al. 1997b, A&AS, 122, 327
Bőttcher, M., et al. 1998, A&A, 343, 111
Castro-Tirado, A.J. et al. 1994, Second Hunstville GRB Workshop, AIP Conf. Proc. 307 (eds: Fishman, G., Brainerd, G. and Hurley, H.), p. 17
Costa, E. et al. 1997, Nature, 387, 783

Cohen, E. et al. 1997, ApJ, 488, 330
Crider, A. et al. 1997, ApJ, 479, L39
Dal Fiume, D. et al. 1999, in preparation
Dermer, C.D., Bőttcher, M., and Chiang, J. 1999, ApJ, 515, L49 (astro-ph/9902306)
Djorgovski, S.G. et al. 1999, GCN #289
Feroci, M. et al. 1997, SPIE Proceedings, 3114, 186
Feroci, M. et al. 1998, A&A, 332, L29
Ford, L.A., et al. 1995, ApJ, 439, 307
Frontera, F., Costa, E., Dal Fiume, D., Feroci, M., Nicastro, L., Orlandini, M., Palazzi, E., and Zavattini, G. 1997, A&AS, 122, 357
Frontera, F. et al. 1998, ApJ, 493, L67
Frontera, F. et al. 1998b, in Proc. Fourth Huntsville Symp. on Gamma-Ray Bursts, ed. C.A. Meegan, R. Preece and T.M. Koshut, AIP Conf. Proc. 428, 446.
Fruchter, A. 1999, ApJ, 512, L1
Galama, T. et al. 1998a, ApJ, L97
Galama, T. et al. 1998b, Nature, 395, 670
Gorosabel, J. et al. 1998, A&A, 339, 719
Groot, P.J., et al. 1998, ApJ, 502, L123
Guidorzi, C. et al. 1998, Nucl. Phys. B (Proc. Suppl), 69, 664
Heise, R., et al. 1998, paper presented at the 192nd AAS Meeting, San Diego, CA
Jager, R., et al. 1997, A&AS, 125, 557
Katz, J., 1994, ApJ, 432, L107
Kobayashi, S., Piran, T. and Sari, R. 1997, ApJ, 490, 92
Kulkarni, S.R. et al. 1998a, Nature, 393, 35
Liang, E.P. et al. 1997, ApJ, 497, L35
Manzo, G., Giarrusso, S., Santangelo, A., et al. 1997, A&AS, 122, 341–356
Masetti, N. et al. 1999, A&AS, 138, 453
Mészáros, P. and Rees, M.J. 1992, ApJ, 397, 570
Mészàros, P., Laguna, P. and Rees, M. J. 1993, ApJ, 415, 181
Mészáros, P. and Rees, M.J. 1997, ApJ, 476, 2
Mészáros, P. and Rees, M.J. 1999, MNRAS, in press (astro-ph/9902367)
Metzger, M.R. et al. 1997, Nature387, 878
Morrison R. and McCammon, D. 1983, ApJ, 270, 119
Murakami, T. et al 1991, Nature350, 592
Nicastro, L. et al. 1998, A&A, 338, L17
Palazzi, E. et al. 1998, A&A, 336, L95
Papathanassiou, H. 1998, A&AS, 138, 525
Parmar, A.N. et al. 1997, A&AS, 122, 309
Pian, E. et al. 1999a, A&AS, 138, 463
Pian, E. et al. 1999b, ApJ, submitted
Piro, L. et al. 1998a, A&A, 329, 906
Piro, L. et al. 1998b, A&A, 331, L41
Preece, R. et al. 1996, ApJ, 473, 310
Preece, R. et al. 1998, ApJ, 506, L23
Ramaprakash, A.N. et al. 1998, Nature, 393, 43
Rybicki, G.B., and Lightman, A.P. 1979, Radiative Processes in Astrophysics (Wiley-Interscience Publ., New York)
Sari, R. and Piran, T. 1997a, ApJ, 485, 270
Sari, R. and Piran, T. 1997b, MNRAS, 287, 110
Sari, R. 1997, ApJ, 489, L37
Sari, R., Piran, T. and Narayan, R. 1998, ApJ, 497, L17
Sari, R. and Piran, T. 1999a, astro-ph/9901338
Sari, R. and Piran, T. 1999b, A&AS, 138, 537
Sahu, K.C. and Sterken, C. 1998, IAU Circ. No. 6808
Strohmayer, T.E., et al. 1998 ApJ, 500, 873
Tavani, M. 1996, ApJ, 466, 768
Tavani, M. 1997, ApJ, 483, L87
Tavani, M. 1999, in preparation.
Vietri, M. 1997, ApJ, 478, L9
Waxman, E 1997, ApJ, 485, L5
Wijers, R.A.M.J., Rees, M.J., and Mészáros, P. 1997, MNRAS, 288, L51
in 't Zand, J. 1998, ApJ, 505, L11

TABLE 1
GRBS INCLUDED IN OUR SAMPLE

GRB	Position error radius	Offset wrt inst. axis	X–ray [a] peak flux	T_x (s)	γ–ray [a] peak flux	T_γ (s)	1^{st} TOO delay	Counterparts
GRB960720	3'	11.1°	0.25	17	10	8	45^d	
GRB970111	3'	14.6°	1.4	60	56	43	16^h	X ?
GRB970228	3'	13.1°	1.4	55	37	80	8^h	X, opt.
GRB970402	3'	8.5°	0.16	150	3.2	150	8^h	X
GRB970508	1.9'	10.3°	0.35	29	5.6	15	5.7^h	X, opt.,radio
GRB971214	3.3'	16.5°	0.2	35	6.8	35	6.7^h	X, opt.
GRB980329	3'	19.2°	1.3	68	51	58	7^h	X, opt., radio
GRB980425	8'	15.1°	0.61	40	2.4	31	9^h	X, opt, radio ?

[a] Peak fluxes in units of 10^{-7} erg cm^{-2} s^{-1}

TABLE 2
SPECTRA OF GRBS AND ASSOCIATED X–RAY AFTERGLOW

#	GRB	Sect.	$-\Gamma_X$ [a]	$-\Gamma_\gamma$ [a]	E_p [b]	N_H [b]	$-\Gamma_a$	$N_{H,a}$	δ	Ref.
1	GRB960720	A	< -0.1	< -0.1	> 700	0.255				
		B	0.39 ± 0.18	0.39 ± 0.18	> 700	0.255				
		C	0.49 ± 0.17	1.76 ± 0.32	178 ± 40	0.255				
		D	0.76 ± 0.21	2.21 ± 0.40	28 ± 17	0.255				
		E	1.18 ± 0.31	> 1.64	< 16.7	0.255				
		F	1.9 ± 0.6	> 2.44	< 3.	0.255	...	...	...	
2	GRB970111	A	< -0.37	0.63 ± 0.33	> 500	0.46				
		B	< -0.4	1.18 ± 0.17	> 194	0.46				
		C	-0.63 ± 0.36	1.23 ± 0.09	> 170	0.46				
		D	-0.92 ± 0.31	1.72 ± 0.06	> 115	0.46				
		E	-0.76 ± 0.39	1.73 ± 0.06	> 118	0.46				
		F	-0.82 ± 0.27	1.89 ± 0.05	> 89	0.46				
		G	-0.96 ± 0.29	2.38 ± 0.11	37 ± 12	0.46				
		H	-0.87 ± 0.27	2.77 ± 0.11	33 ± 8	0.46				
		I	-0.19 ± 0.17	2.9 ± 0.2	36 ± 9	0.46				
		J	0.33 ± 0.12	3.05 ± 0.27	35 ± 7	0.46	...	...	> 1.5	(1)
3	GRB970228	A	0.92 ± 0.03	1.54 ± 0.18	> 700	1.6				
		B	1.4 ± 0.1	2.5 ± 0.1	35 ± 18	1.6				
		C	1.8 ± 0.1	1.8 ± 0.1	< 2	1.6				
		D	1.84 ± 0.09	1.84 ± 0.09	< 2	1.6				
		E	1.92 ± 0.15	1.92 ± 0.15	< 2	1.6				
		F	1.5 ± 0.4	> 0.6	< 2	1.6				
		G	1.6 ± 0.1	1.4 ± 0.3	< 2	1.6	2.06 ± 0.24	3.5 ± 2.3	1.33 ± 0.12	(2)
4	GRB970402	A	1.38 ± 0.03	1.38 ± 0.03	≥700	< 20				
		B	1.36 ± 0.04	1.36 ± 0.04	≥700	2.1	1.7 ± 0.6	2.1	1.56 ± 0.03	(3)
5	GRB970508	A	0.83 ± 0.11	0.83 ± 0.11	> 700	0.51				
		B	1.54 ± 0.10	1.54 ± 0.10	≥700	0.51				
		C	1.74 ± 0.14	1.74 ± 0.14	≥700	0.51				
		D	1.8 ± 0.4	> 1.4	< 24	0.51	2.1 ± 0.6	10. ± 5.	1.1 ± 0.1	(4),(5)
6	GRB971214	A	0.37 ± 0.23	1.4 ± 0.03	> 700	0.16				
		B	0.33 ± 0.27	1.0 ± 0.07	> 224	0.16				
		C	0.96 ± 0.09	2.6 ± 0.5	56 ± 10	0.16	1.7 ± 0. 2	0.9 ± 0.5	1.2 ± 0.13	(6),(7)
7	GRB980329	A	< 0.16	1.32 ± 0.03	> 229	120 ± 80				
		B	0. ± 0.33	1.30 ± 0.06	> 168	120 ± 80				
		C	0.36 ± 0.19	1.25 ± 0.08	> 210	120 ± 80				
		D	0.67 ± 0.11	1.29 ± 0.02	> 320	120 ± 80				
		E	0.73 ± 0.18	1.61 ± 0.04	> 213	250 ± 100				
		F	0.78 ± 0.32	1.70 ± 0.09	> 180	85 ± 40				
		G	1.0 ± 0.4	1.7 ± 0.2	> 175	10.				
		H	1.5 ± 0.5	2.3 ± 0.3	105 ± 80.	10.	2.4 ± 0.4	10 ± 0.4	1.35 ± 0.03	(8)
8	GRB980425	A	< 0.3	1.75 ± 0.15	> 68	0.396				
		B	0.78 ± 0.27	2.3 ± 0.1	68 ± 40	0.396				
		C	1.45 ± 0.75	3.3 ± 0.7	31 ± 25	0.396				
		D	1.6 ± 0.5	> 3.8	< 57	0.396	...	...	>1.3	(9)

[1]Feroci et al. 1998 , [2]Frontera et al. 1998 , [3]Nicastro et al. 1998 , [4]Piro et al. 1998 , [5]Amati et al. 1998 , [6]Heise et al. 1998 , [7]Dal Fiume et al. 1999, [8]in 't Zand et al. 1998 , [9]Pian et al. 1999a

[a]The photon indices reported in columns 2 and 3 refer to fit with the smoothed broken power-law proposed by Band et al. (1993)

[b]E_p values are in keV; N_H values are in units of $10^{21}\ cm^{-2}$

[c]Data referring to the first impulse of the event (see text and paper from Frontera et al. 1998a)

TABLE 3
GRB AND X–RAY AFTERGLOW ENERGETICS [a]

GRB	S_X (2–10 keV)	S_γ (40–700 keV)	S_a (2–10 keV)	S_X/S_γ (%)	S_a/S_γ (%)	S_a/S_X	E_{52} [b]	z	Ref. [c]
GRB960720	0.08 ± 0.02	2.6 ± 0.3		3.0 ± 0.8	···	···	···	···	···
GRB970111	1.6 ± 0.1	43 ± 3.	< 1.1	3.7 ± 0.2	< 3	< 0.69	···	···	···
GRB970228	2.2 ± 0.5	11 ± 1.	2.16 ± 0.81	20 ± 0.81	19.6 ± 0.2	0.98 ± 0.19	0.25	0.695	(1)
GRB970402	0.4 ± 0.04	8.2 ± 0.9	0.47 ± 0.15	4.8 ± 0.1	5.7 ± 0.7	1.17 ± 0.13			
GRB970508	0.33 ± 0.05	1.8 ± 0.3	0.47 ± 0.31	38.9 ± 1.8	26 ± 12	0.67 ± 0.30	∼0.078	0.835	(2)
GRB971214	0.19 ± 0.03	8.8 ± 0.9	0.35 ± 0.14	1.2 ± 0.1	3.9 ± 0.7	3.20 ± 0.75	∼0.936	3.418	(3)
GRB980329	0.7 ± 0.12	55. ± 5.	0.72 ± 0.27	1.0 ± 0.04	0.40 ± 0.07	0.39 ± 0.8	∼3.86 (?)	∼ 5 (?)	(4)
GRB980425	0.78 ± 0.02	2.8. ± 0.5	<0.46	28 ± 5	<16	<0.59	$< 7.45\text{x}10^{-6}$	0.008	(5)

[a] All fluences are given in units of 10^{-6} erg/cm^2

[b] E_{52} = afterglow energy in units of 10^{52} erg

[c] References for redshift: [1]Djorgovski et al., 1999 , [2]Metzger et al., 1997 , [3]Kulkarni et al. 1998a , [4]Fruchter, 1999 , [5]Galama et al., 1998b

TABLE 4

Derivation of external shock physical parameters

GRB	t_0(s) ad	t_0(s) rad	γ_0	ϵ_B(early) ad	ϵ_B(early) rad	ϵ_e(early) ad	ϵ_e(early) rad	$F_{\nu,max}$(early) (mJy)	ϵ_B(late)	$F_{\nu,max}$(late)[a] (mJy)	p[b] (t_m<t<t_c)	p[b] (t>t_c)
GRB970228	42	42	110	0.005	0.0052	0.61	0.63	> 10	0.001	?	2.77	2.44
GRB970508	1000	550	181±120	0.046	···	0.57	···	> 1	0.037	~ 2	2.13	2.46
GRB971214	$\sim$1x10^4	$\sim$3x10^4	180±78	···	0.15	···	0.65	~ 0.3	···	0.02−0.09	2.27	2.60
GRB980329	$\sim$6.9x10^5	1.5x10^5	215±80[c]	0.053	···	$\sim$1	···	$\sim$0.35	0.071	$\sim$0.3	2.47	2.80
GRB980425	···		<50	···		···		···	···	···	···	

[a]References for $F_{\nu,max}$(late): Masetti et al. 1999 (GRB970228), Galama et al. 1998a (GRB970508), Dal Fiume et al. 1999 and Ramaprakash et al. 1998 (GRB971214), Palazzi et al. 1998 (GRB980329)

[b]The typical error on the reported p values is 0.15

[c]Assuming the redshift proposed by Fruchter 1999

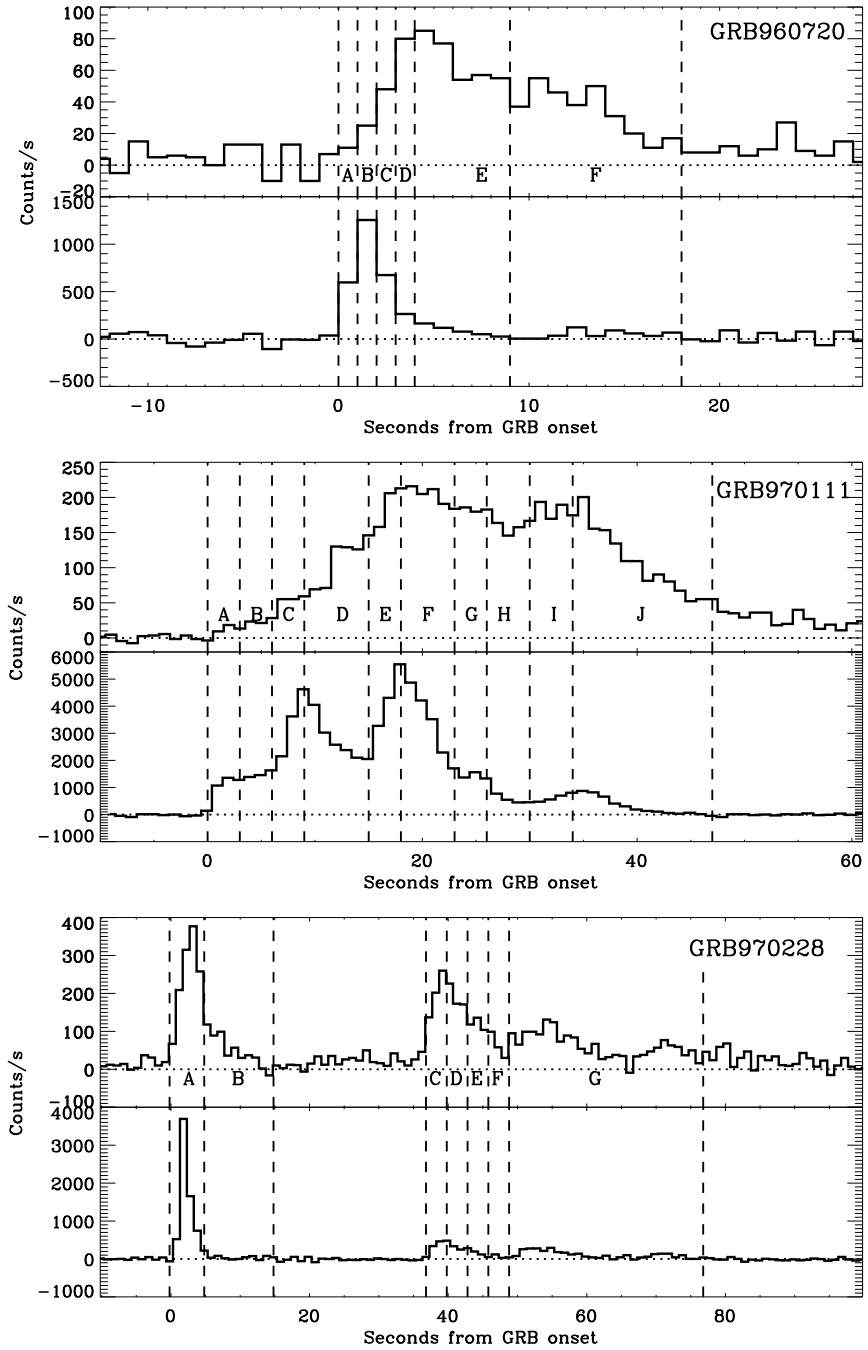

FIG. 1.— Light curves of GRBs in our sample, after background subtraction, in the 2–26 keV (upper panels) and 40–700 keV (lower panels) energy bands. Horizontal dotted line gives the background reference of each GRB. Vertical dashed lines indicate the temporal sections in which we performed the spectral analysis.

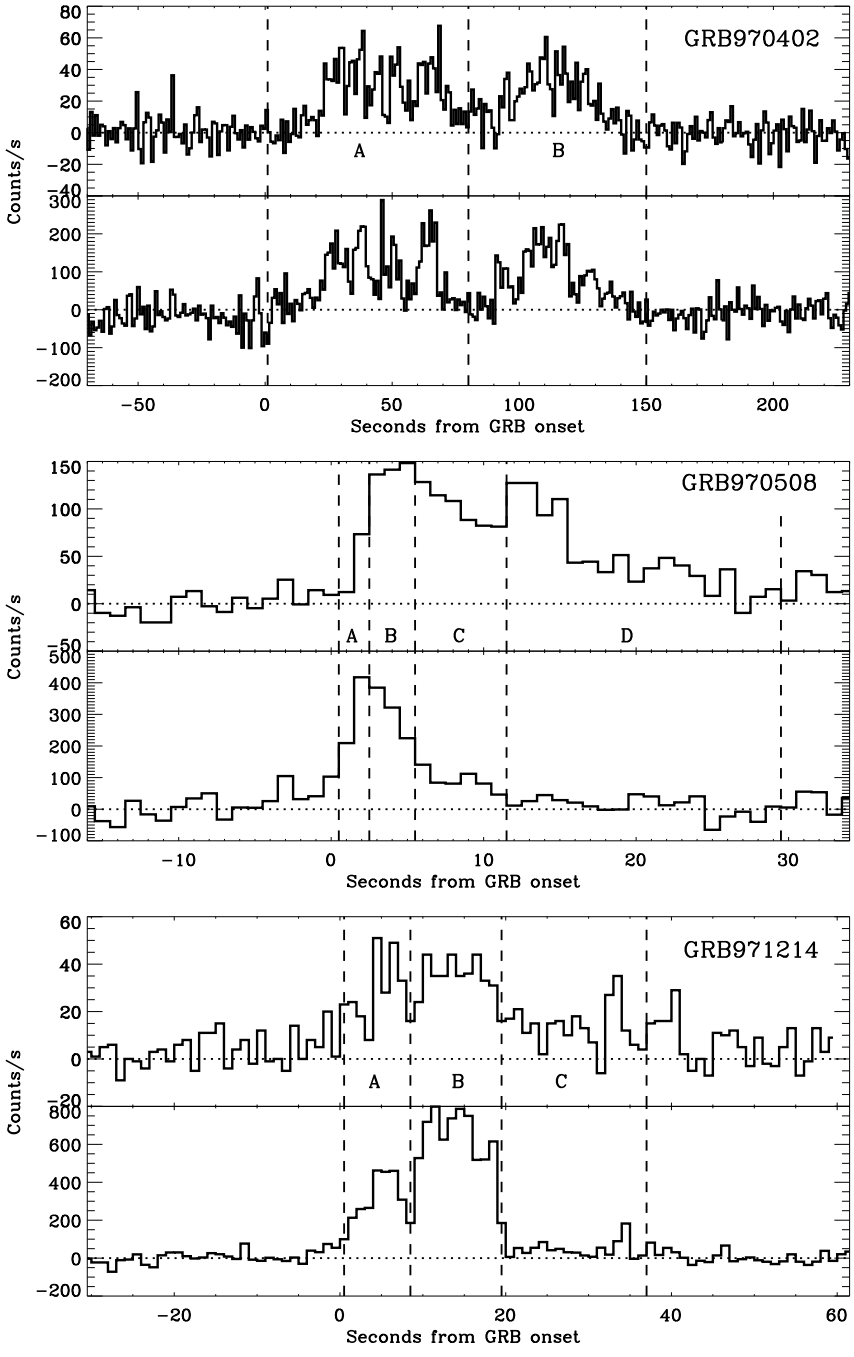

FIG. 1–CONTINUED.—

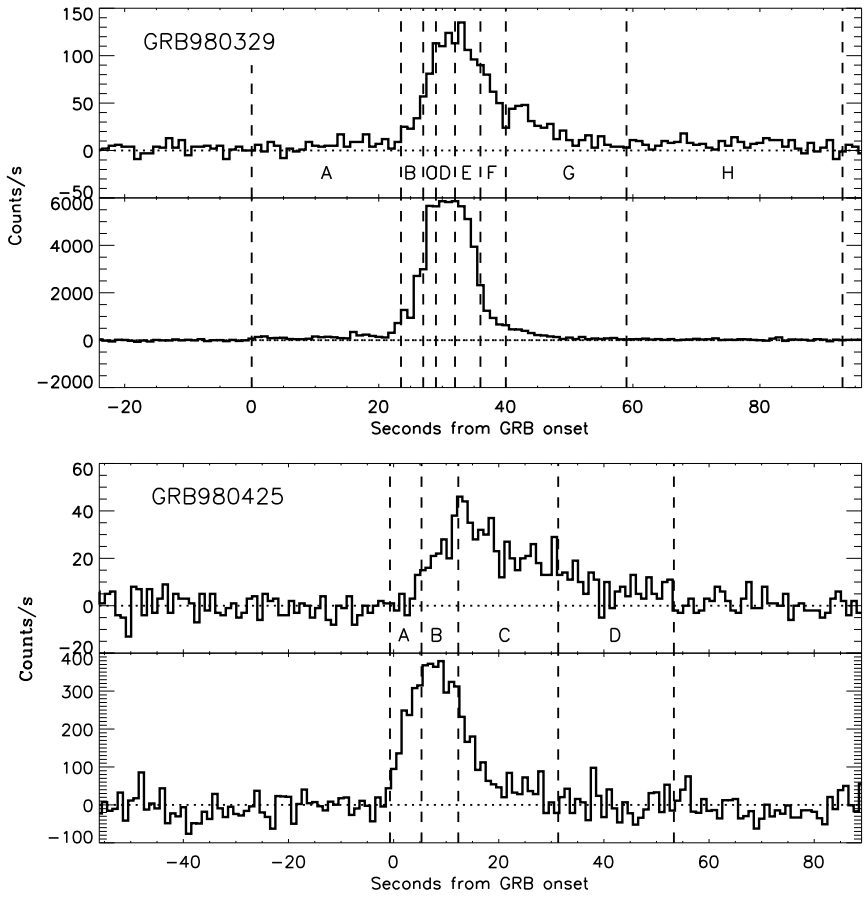

FIG. 1–CONTINUED.—

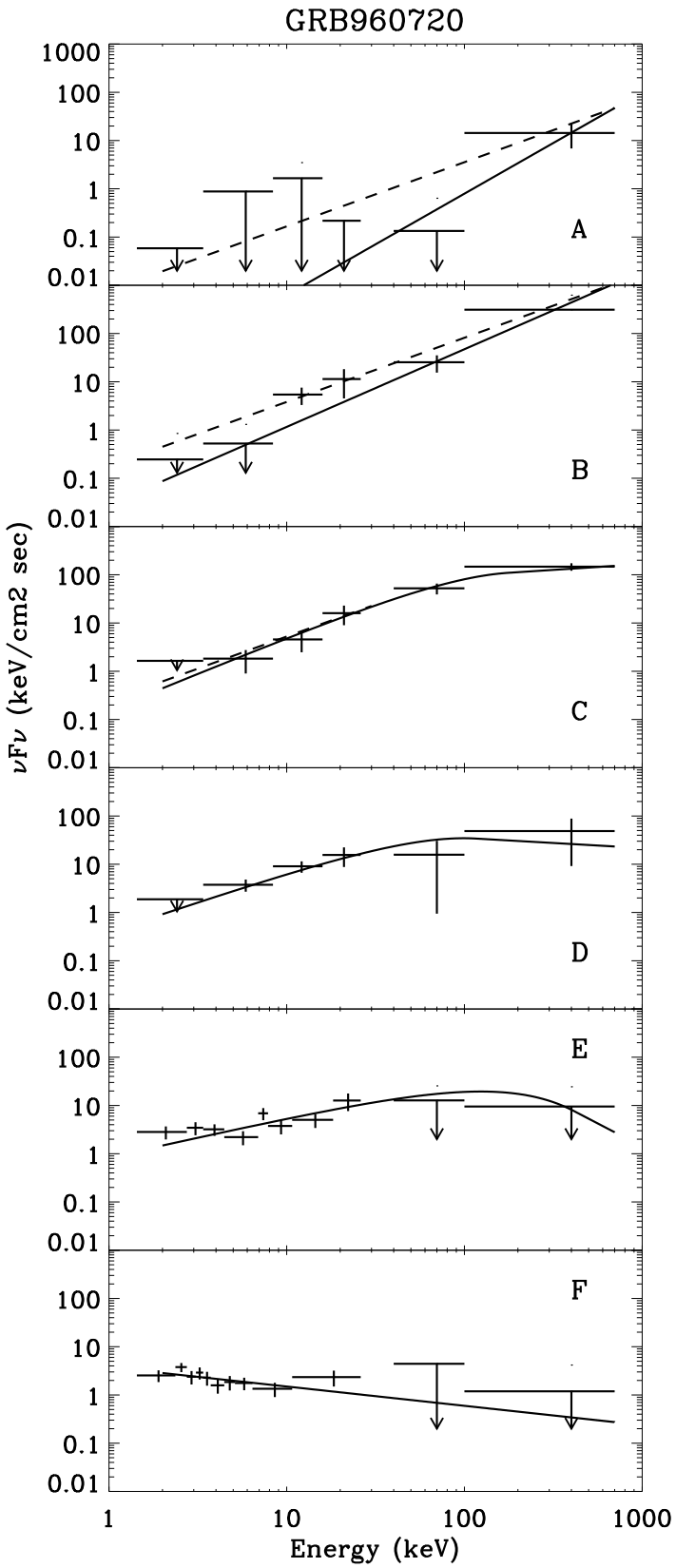

FIG. 2.— Spectral energy distributions ($\nu F(\nu)$) of GRBs in the 2–700 keV. For each GRB, in the different panels are reported the spectra in the temporal sections in which we divided the GRB light curve. Solid lines give the best fit of the Band law (Band et al. 1993) to the data. Dashed lines show the limit slope in the case of an optically thin synchrotron model (see text).

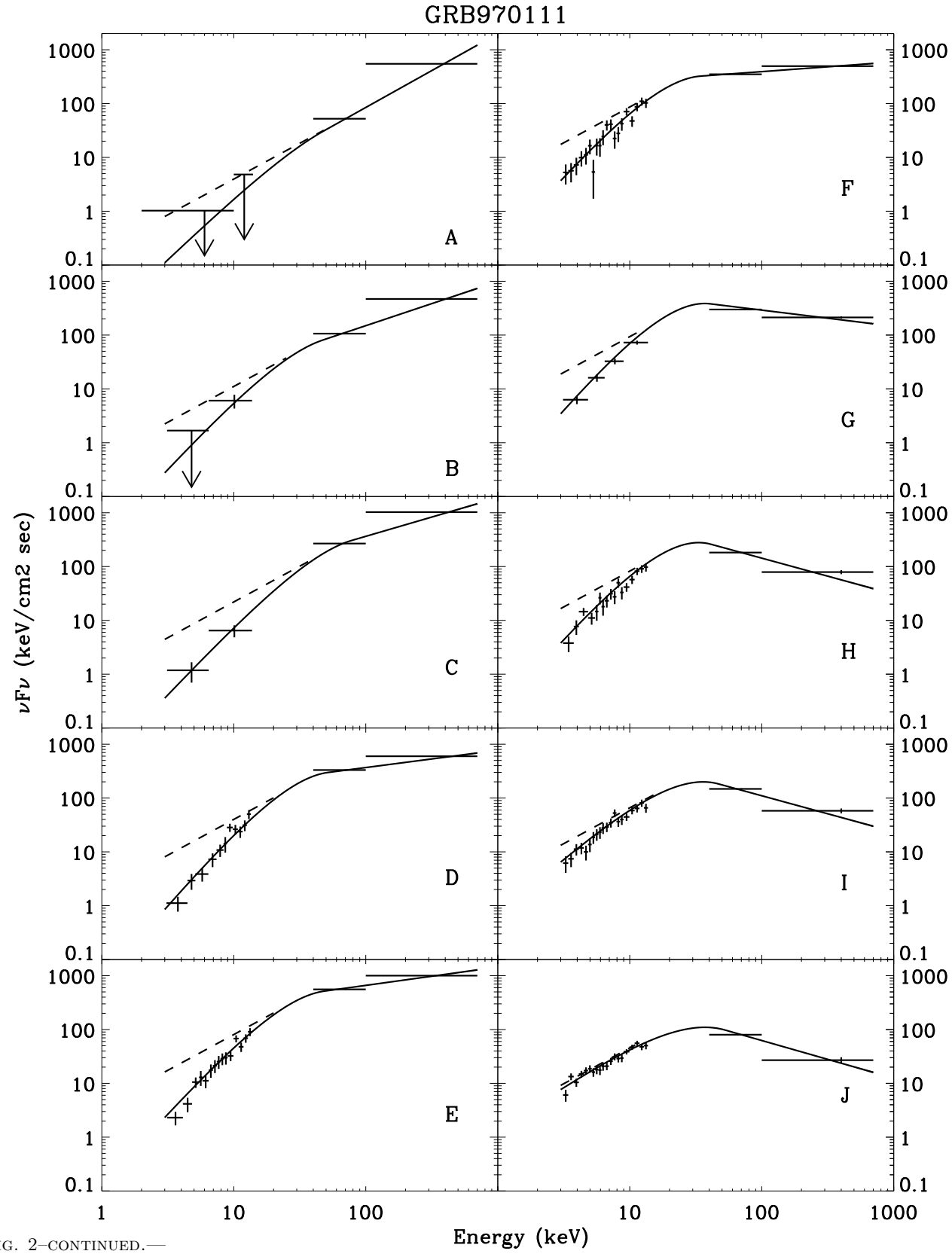

FIG. 2–CONTINUED.—

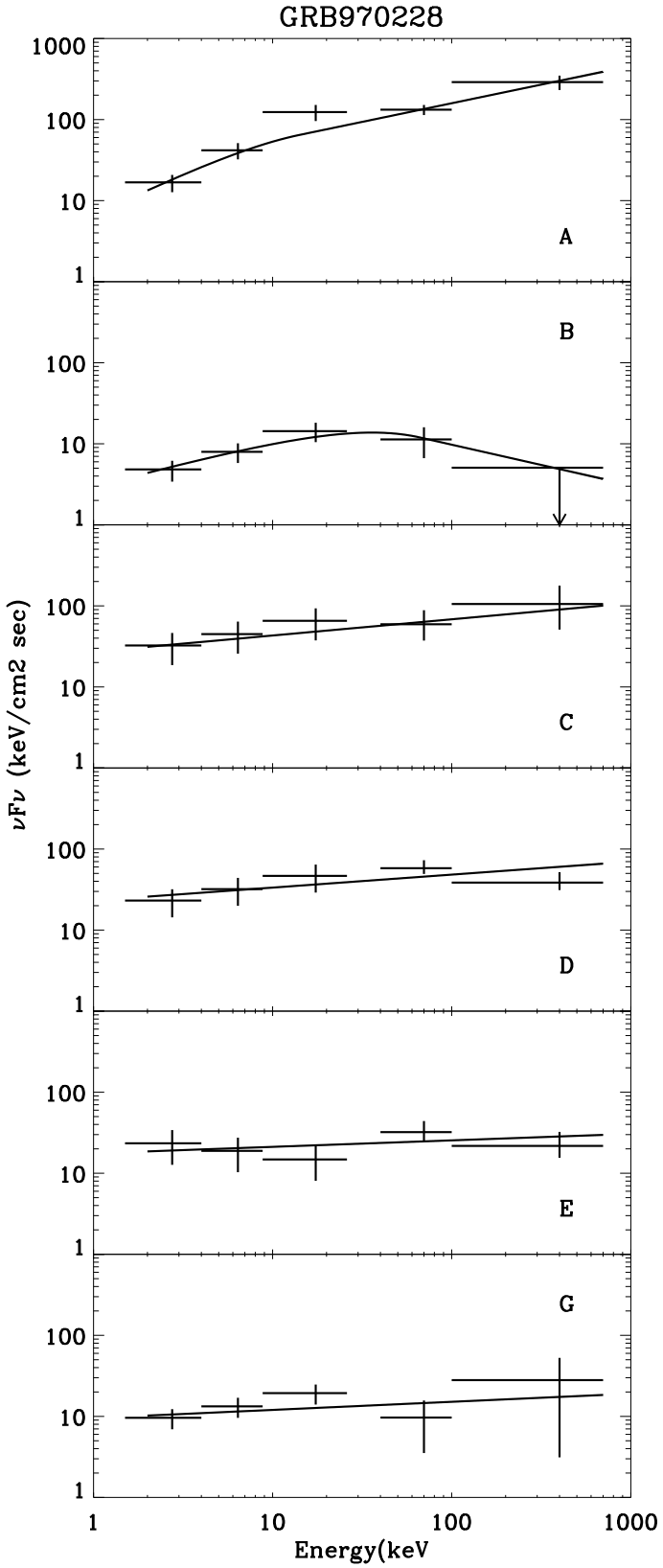

FIG. 2–CONTINUED.—

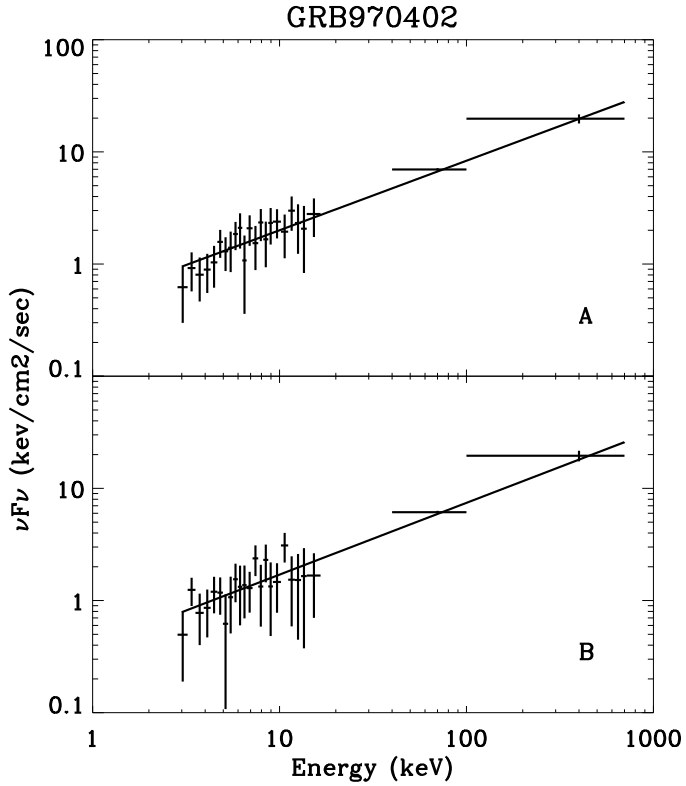

FIG. 2–CONTINUED.—

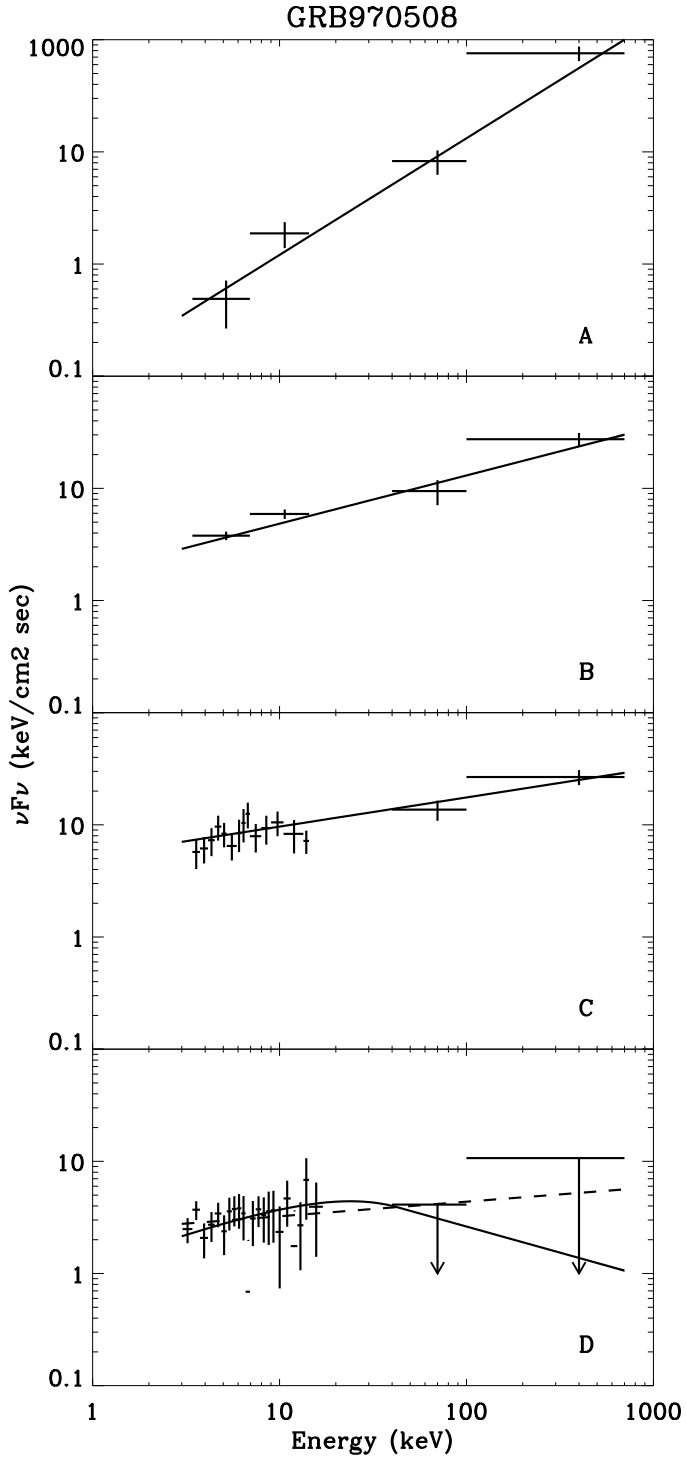

FIG. 2–CONTINUED.—

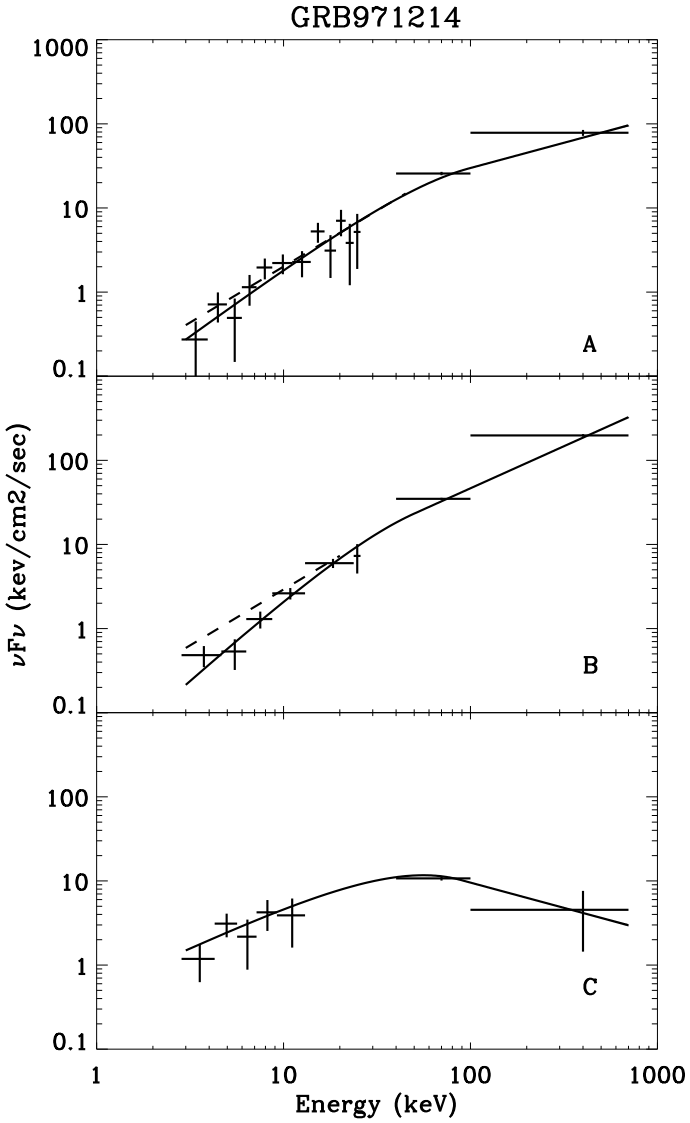

FIG. 2–CONTINUED.—

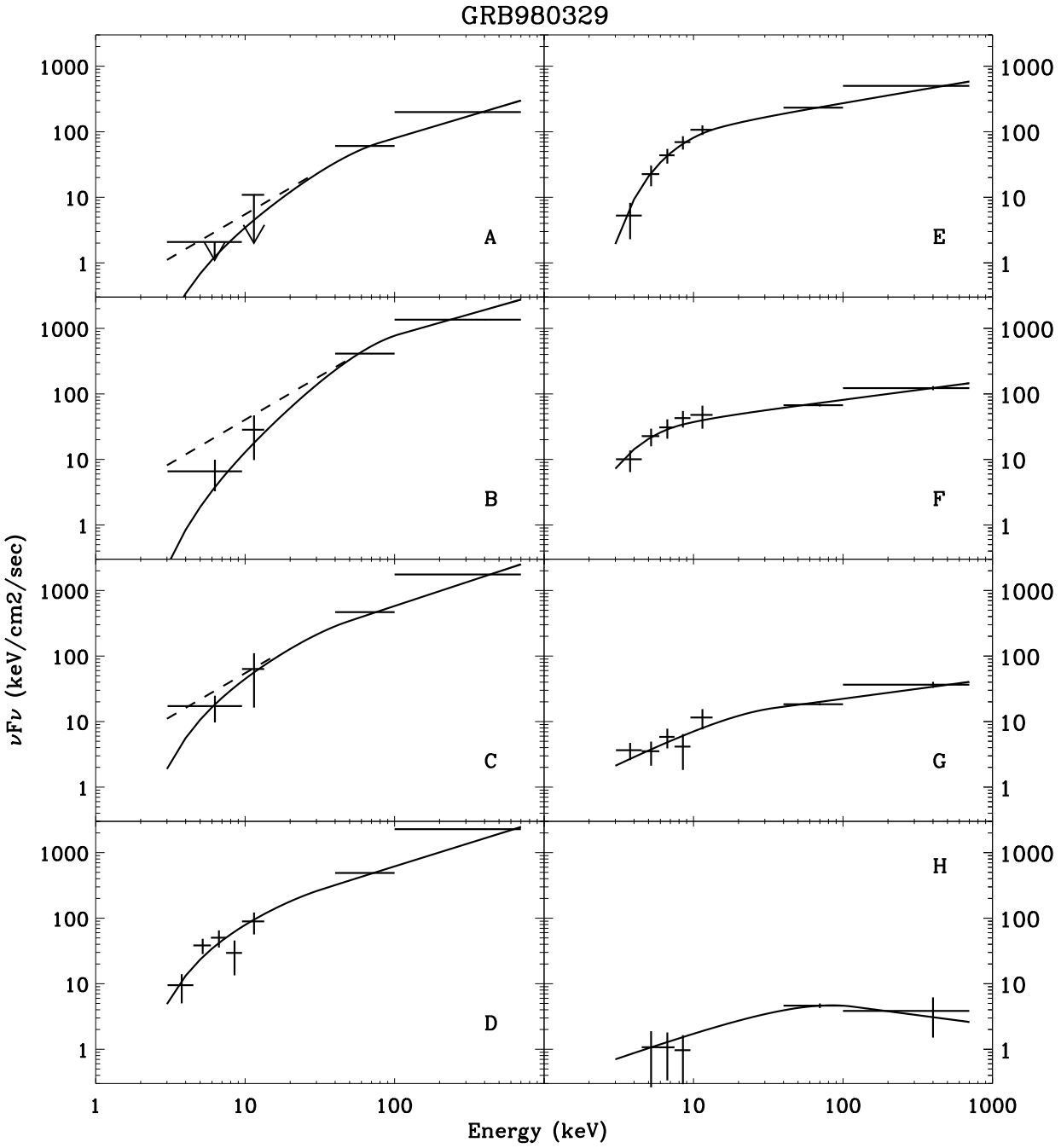

FIG. 2–CONTINUED.—

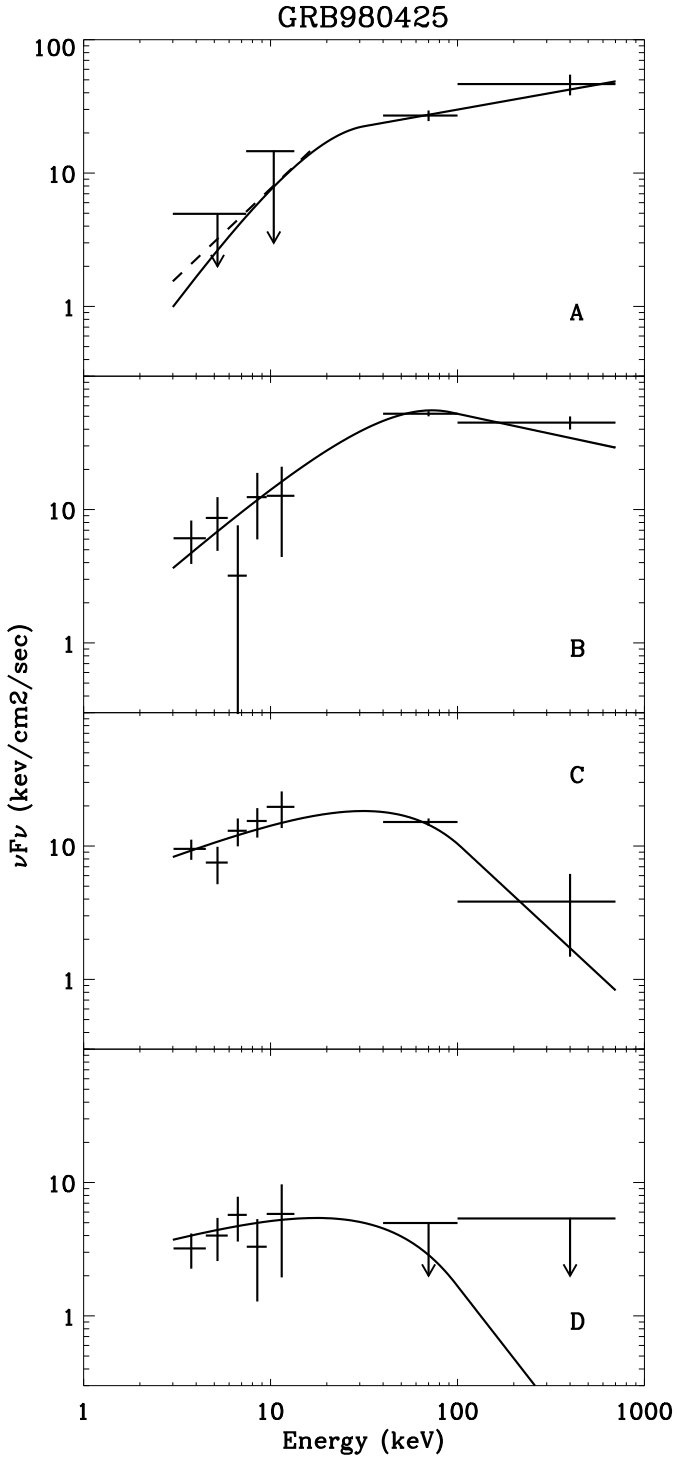

FIG. 2–CONTINUED.—

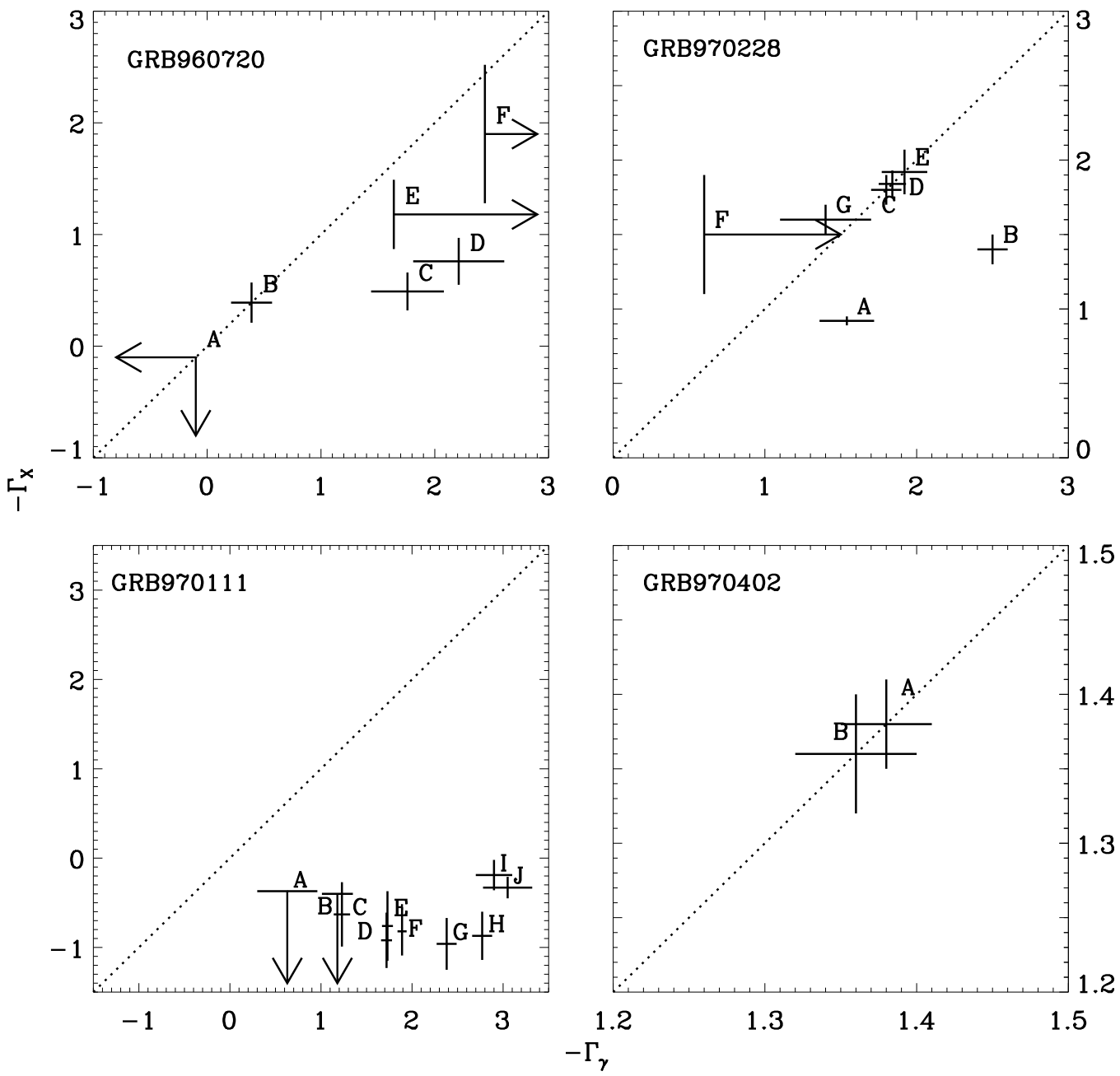

FIG. 3.— Scatter plot of γ–ray photon index (Γ_γ) vs. X–ray photon index (Γ_X). The dashed line shows the locus of $\Gamma_\gamma = \Gamma_X$ (see text).

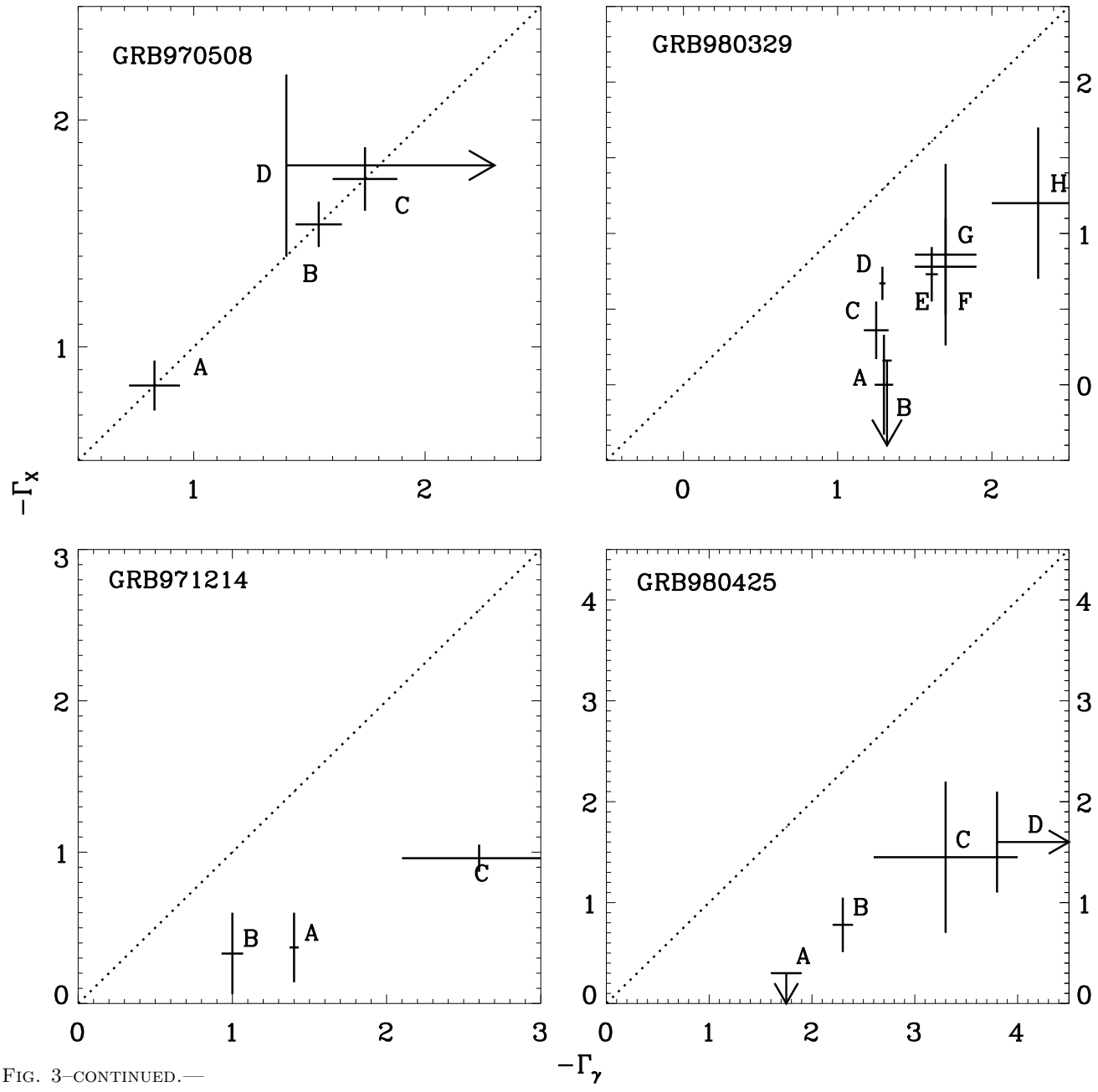

FIG. 3–CONTINUED.—

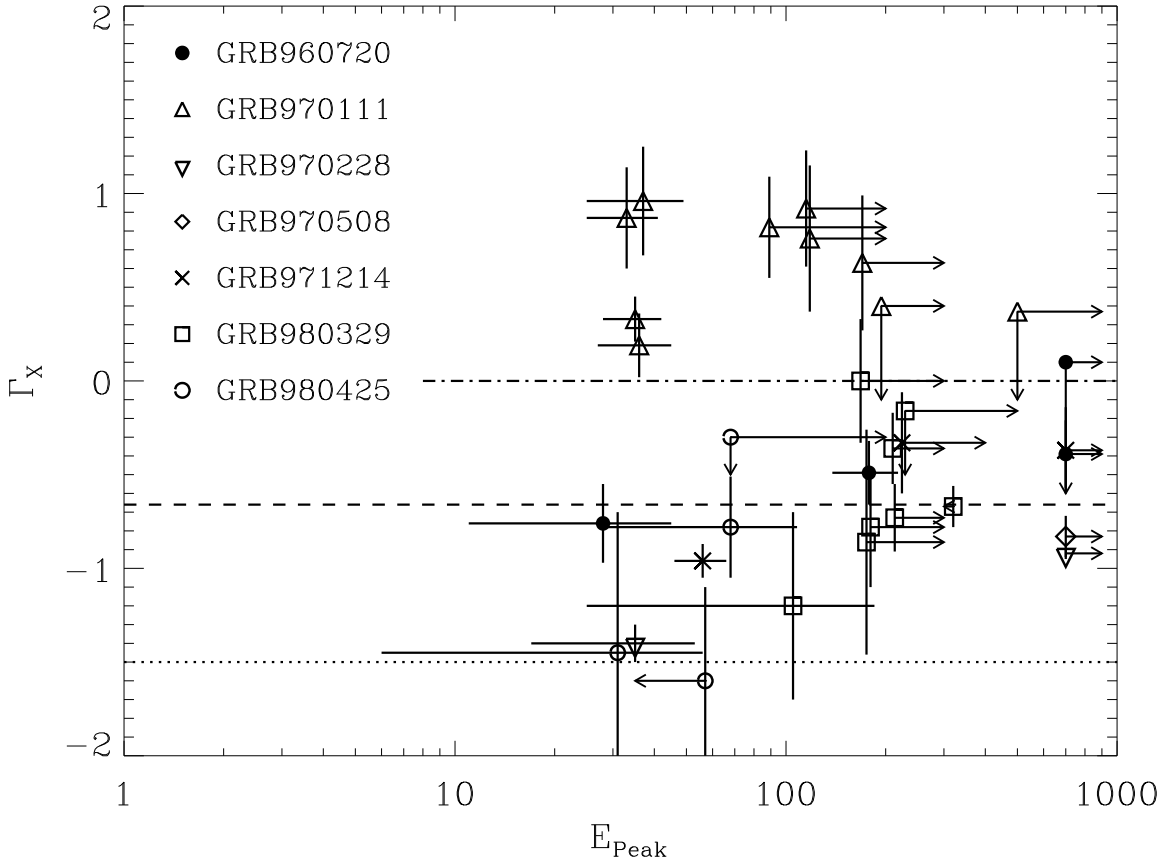

FIG. 4.— Low-energy power law index Γ_X vs. peak energy E_p of the $\nu F(\nu)$ spectrum, for each of the temporal sections of GRBs in our sample. The dashed line corresponds to the maximum power law photon index below the energy break, that is consistent with an optically thin synchrotron shock model, while the dotted line corresponds to the power law index when cooling of the high energy electrons is taken into account (see text). The dashed-dotted line correponds to the limit photon index of the Inverse Compton (see text).

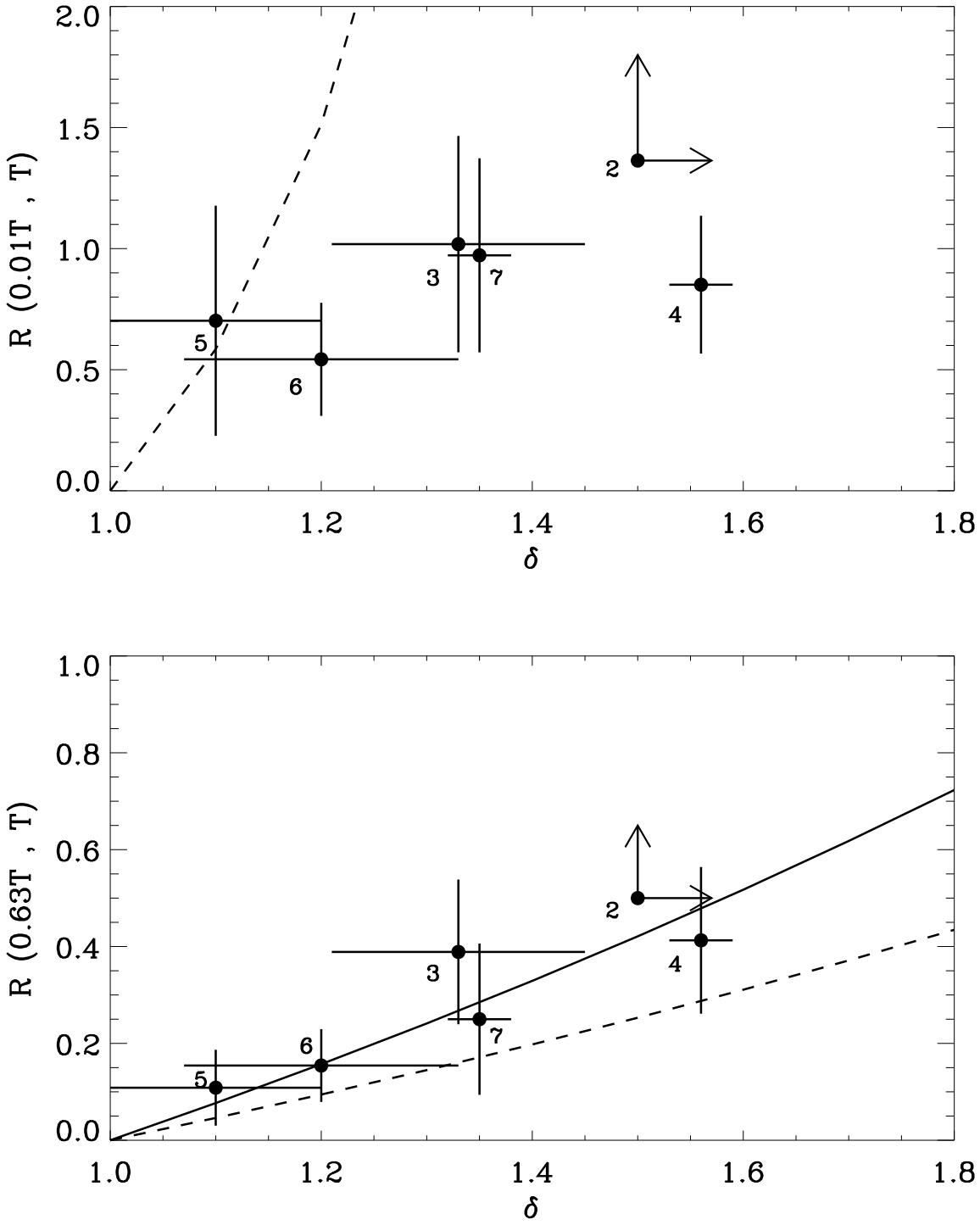

FIG. 5.— Ratio between the 2-10 keV fluence derived from the GRB light curve (*GRB fluence*) and that derived from the late afterglow observation (*afterglow fluence*) vs. the temporal index δ of the late afterglow fading law. The afterglow fluence is integrated from the end (T) of the GRB light curve, as estimated by our data (see Table 1) to 10^6 s (see text).
Top: The GRB fluence is integrated over the time interval starting from 1% of the GRB time duration to its end.
Bottom: The GRB fluence is integrated over the time interval starting from 63% of the GRB time duration and the end of the event.
Superposed to the data are the expected ratios assuming the GRB fluence has the same origin as the late afterglow emission. *Continuous line*: best fit curve; *dashed line*: expected curve if there is no spectral softening from the prompt to the late afterglow emission. The best fit curve in the *top* case would require a hardening of the spectra that is in contrast with the observations.

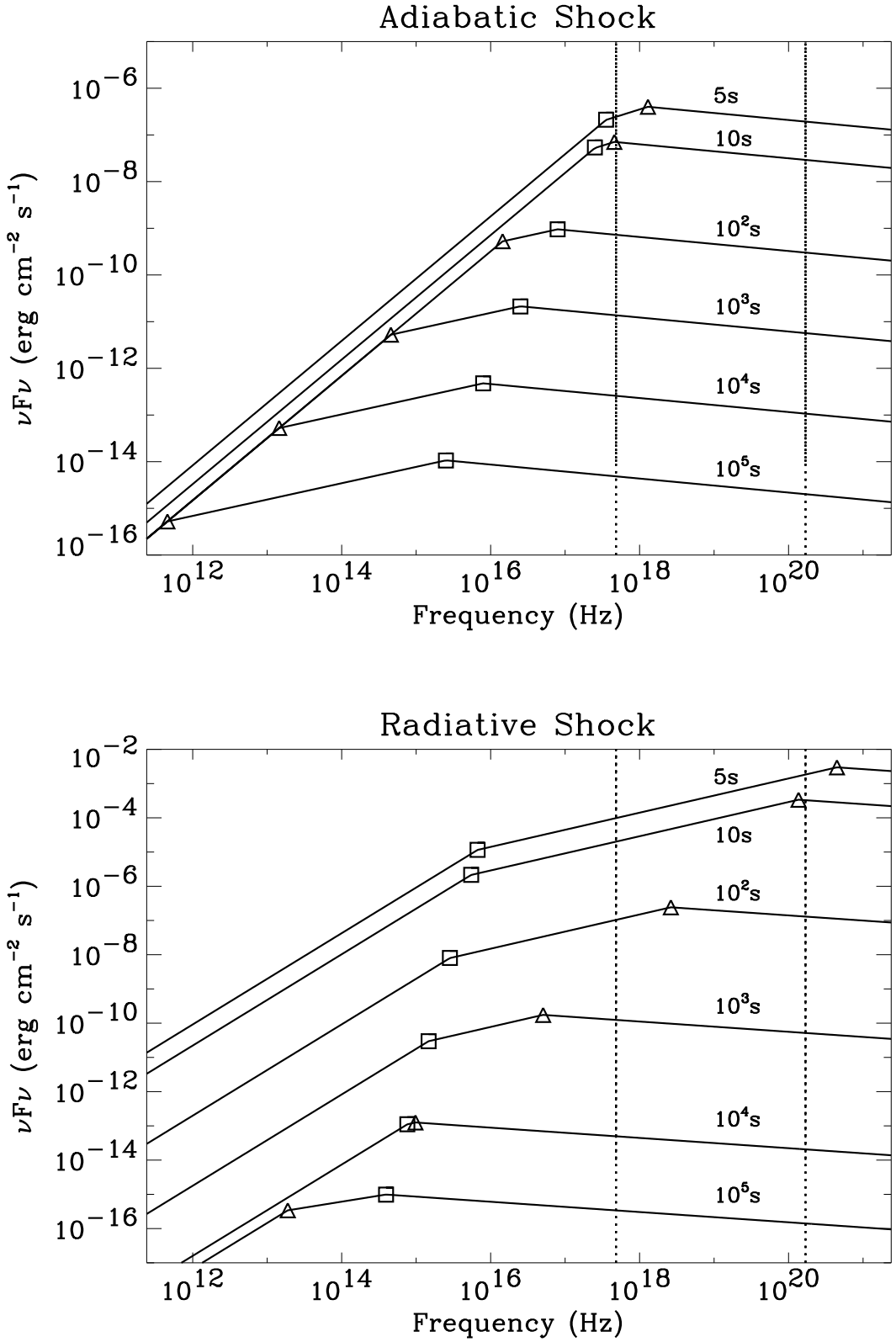

FIG. 6.— Theoretical afterglow spectra at various times from the afterglow onset, expected on the basis of the synchrotron shock model by Sari, Piran and Narayan (1998). *Top*: a fully adiabatic shock; *bottom*: a fully radiative shock. Triangles correspond to the break energy E_m, while the squares correspond to the cooling break E_c (see text for definitions). The dotted vertical lines limit our energy passband. The parameters assumed are: energy of the shock $E = 10^{52}$ erg, index of the power-law distribution of the electrons p = 2.3, particle density of the interstellar medium n = 1 cm^{-3}, fireball distance $D = 10^{28}$ cm, initial Lorentz factor of the ejecta γ_0 =100. The other parameters (see text) ϵ_e and ϵ_B depend on the type of cooling of the shock. We have assumed $\epsilon_B = 0.01$ and $\epsilon_e = 0.1$ for an *adiabatic shock*, $\epsilon_B = 0.1$ and $\epsilon_e = 0.8$ for a *radiative shock*.

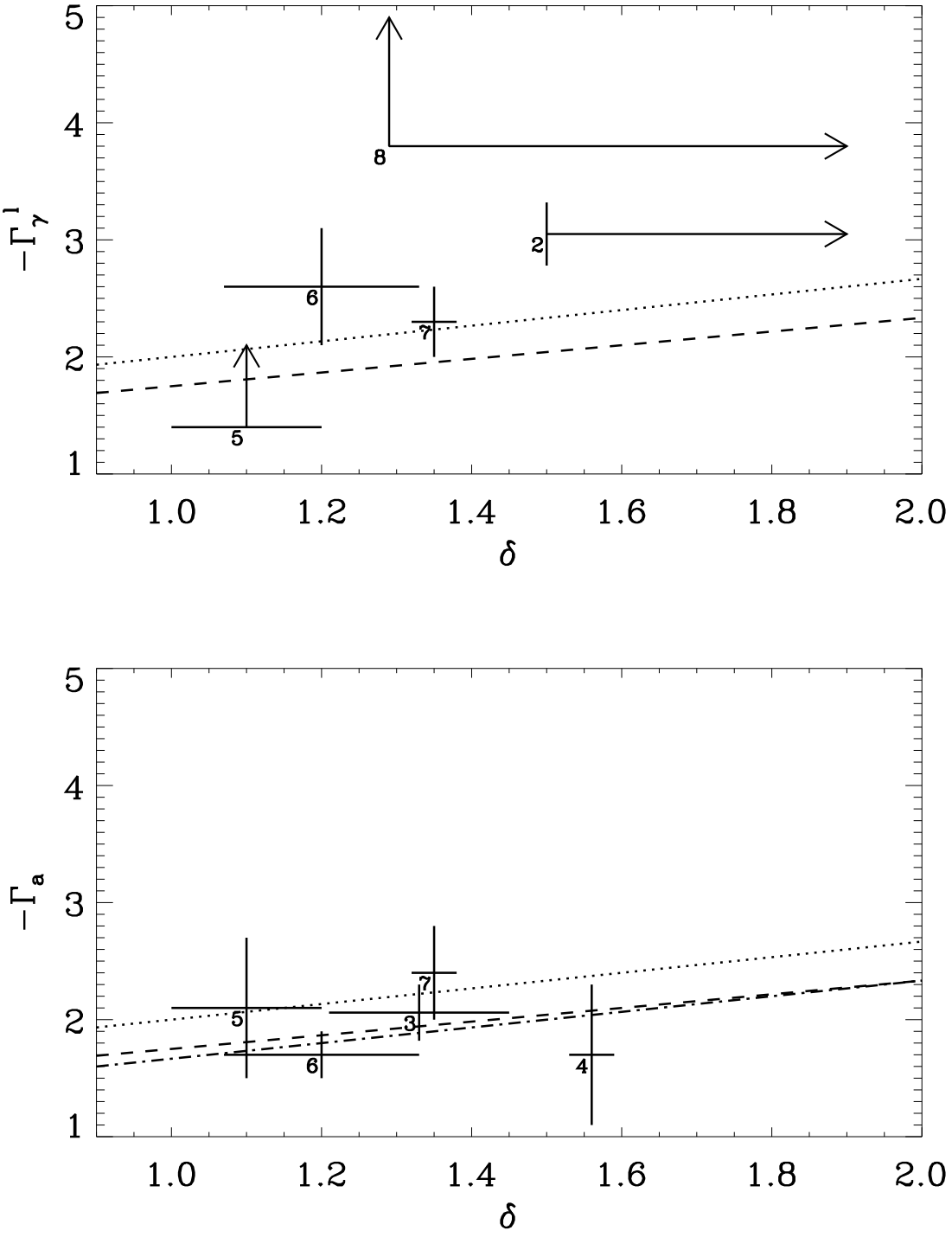

FIG. 7.— *Top panel:* High-energy power-law photon index Γ_γ^l during the GRB tail vs. index of the afterglow fading power-law. *Bottom panel:* photon index Γ_a of the power law spectrum of the X-ray afterglow vs. index of the afterglow fading power-law. *Dotted line*: expected relationship for a fully adiabatic shock if the afterglow observation is performed at time $t>t_c$; *Dotted-dashed line*: expected relationship for a fully adiabatic shock if the afterglow observation is performed at time t, with $t_m < t < t_c$; *Dashed line*: expected relationship for a fully radiative shock. See also text.

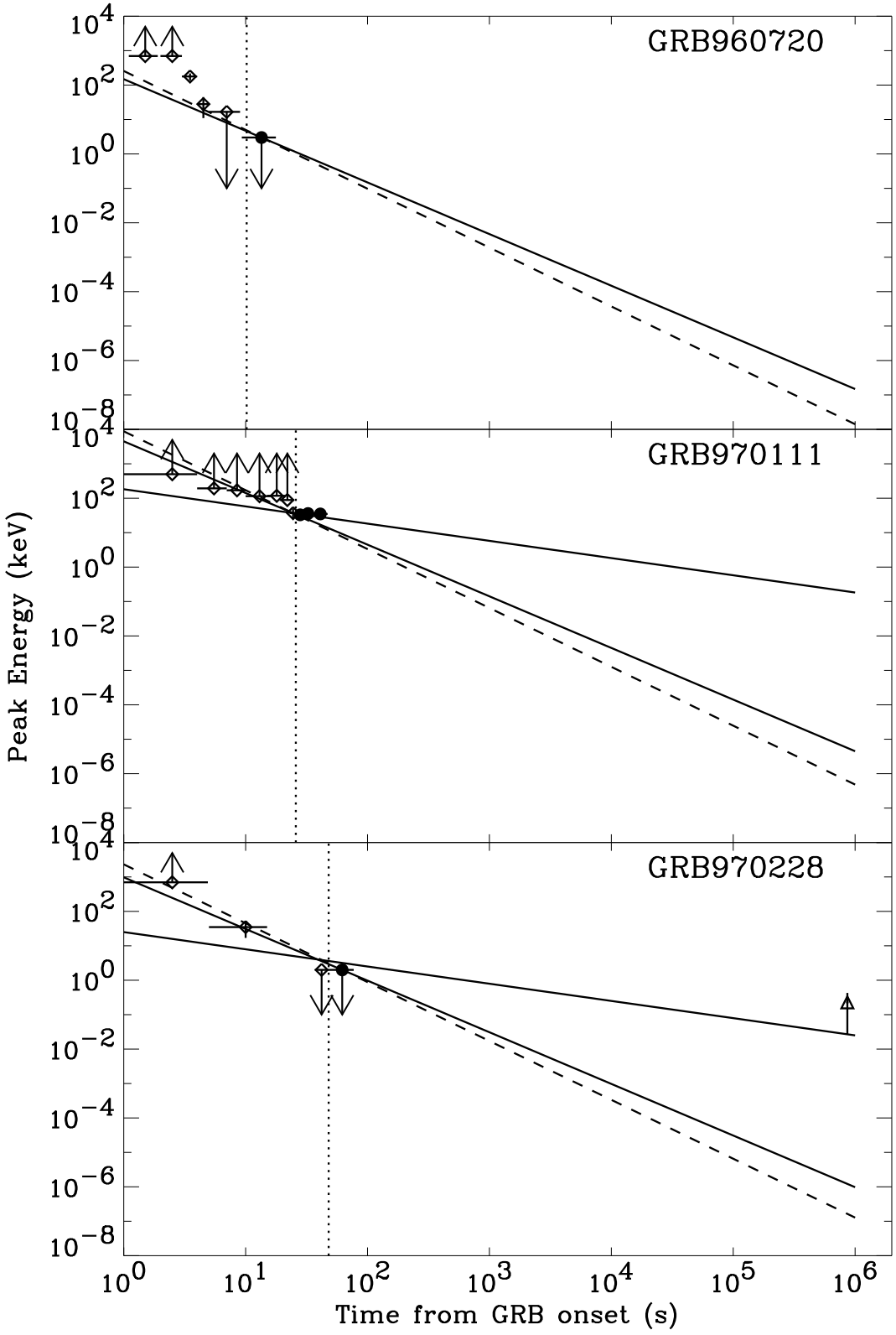

FIG. 8.— Time behaviour of the measured peak energy E_p of the $\nu F(\nu)$ spectrum for GRBs in our sample. *Vertical dotted line*: time at which early afterglow is expected to have already started (see Sect.5.2). E_p values that are expected to be coincident with E_m are shown as *full circles*, while those coincident with E_c are shown with *open triangles*. The expected time behaviour of E_p in the case of the synchrotron shock model by Sari, Piran and Narayan (1998) is also shown for two solutions of the shock: adiabatic (continuum lines) and radiative (dashed lines) cooling. Line with higher slope corresponds to fast cooling and that with lower slope corresponds to slow cooling. See text for details.

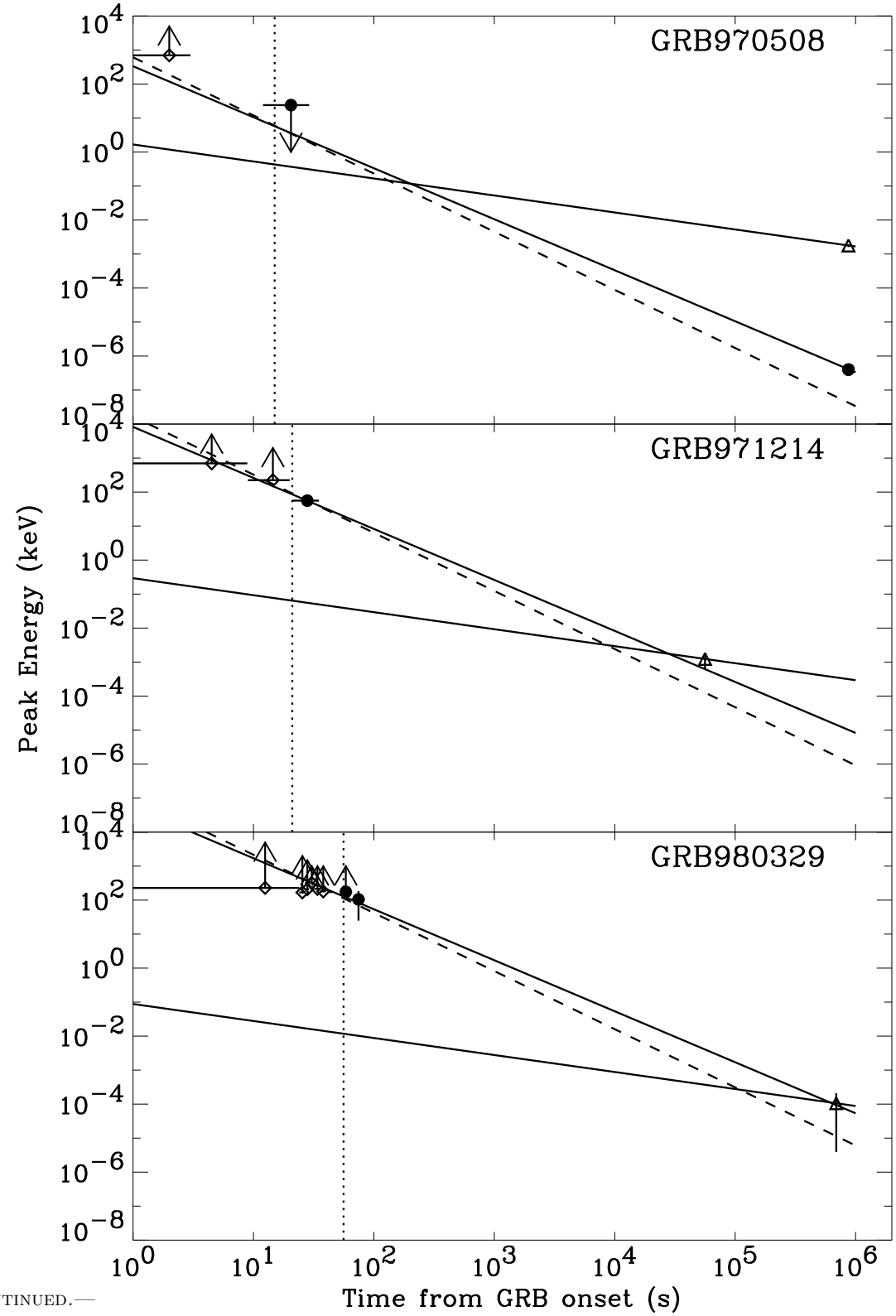

FIG. 8–CONTINUED.—

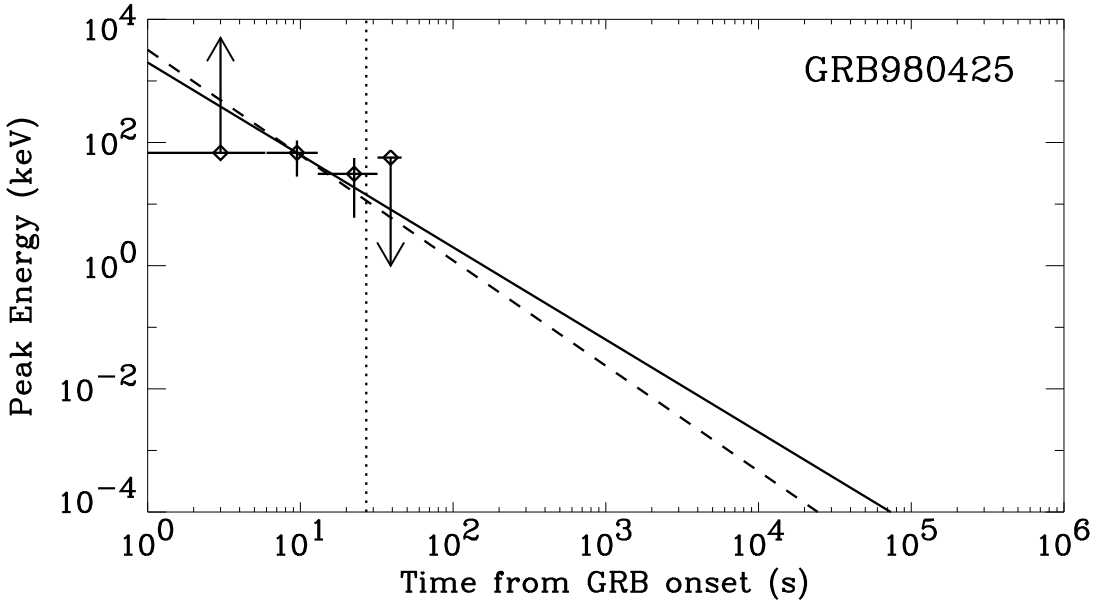

FIG. 8–CONTINUED.—